MODELLING THE AUTONOMIC CARDIAC REGULATION:
INVESTIGATING THE CARDIAC SYMPATHETIC TONE DURING THE VALSALVA MANOEUVRE IN HEALTHY PARTICIPANTS

EEFKE KRIJNEN

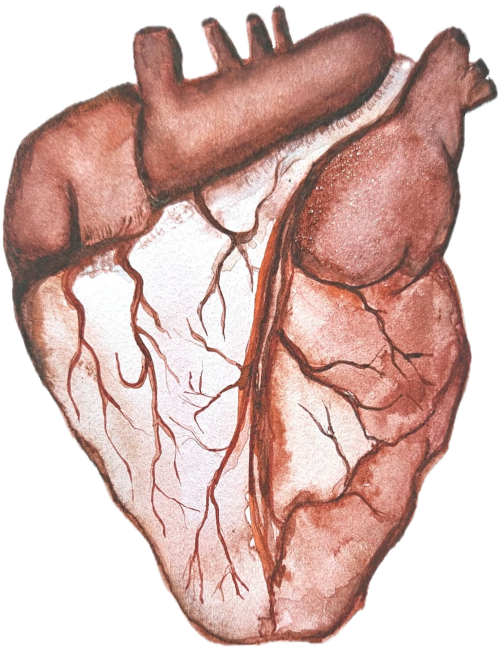

UNIVERSITY OF TWENTE.

MASTER OF SCIENCE THESIS

Biomedical Engineering
Master student Biomedical Engineering
Biomedical Signals and Systems
Electrical Engineering, Mathematics and Computer Science
University of Twente

2024

MASTER GRADUATION COMMITTEE

Chairman:	Prof. Dr. Goos Laverman
Supervisor:	Ying Wang, PhD
Daily supervisor:	Runwei Lin, PhD Candidate
External members:	Prof. Dr. Dirk Donker
	Dr. Frank Halfwerk

CHAIR

Biomedical Signals and Systems

Faculty of Electrical Engineering, Mathematics and Computer Science

University of Twente

E-mail:
eefke.krijnen@gmail.com

This thesis was typeset using a LaTeX template created by André Miede and Ivo Pletikosic in 2018. The template, 'A Classic Thesis Style – An Homage to The Elements of Typographic Style', is available at https://www.ctan.org/tex-archive/macros/latex/contrib/classicthesis/.

The heart illustration on the cover was created by Dian Bonestroo and used with permission.

ABSTRACT

Introduction Autonomic Nervous System (ANS) disorders and cardiac problems are often interrelated. The ANS controls heart rate and maintains homeostasis of blood pressure. This study aimed to evaluate the Sympathetic Nervous System (SNS) using a novel method, Sympathetic Skin Nerve Activity (SKNA) (measured using conventional Electrocardiography (ECG) electrodes). The research identified a gap in simplified, explainable models that simulate the Heart Rate (HR), average Skin Sympathetic Nerve Activity (aSKNA), and Electrodermal activity (EDA) response to the Valsalva Manoeuvre (VM). Therefore, we aimed to create an explainable model to better understand autonomic cardiac regulation.

Objectives The primary goal was to create an explainable mathematical model of autonomic cardiac regulation and its response to the VM, specifically simulating HR, aSKNA, and EDA. The objective was to train the model on experimental data. The hypothesis was that this model could enhance understanding of the ANS and its role in cardiac function, with the simulated features expected to closely resemble experimental data.

Method An exploratory study was conducted in 2024 at the eHealth House at the University of Twente with ten healthy subjects. Additionally, the dataset of Study 2023, earlier obtained by Tertoolen[1] was employed. A simplified model was developed, encompassing baroreceptors, the ANS, the cardiovascular system, and the skin. The model simulated HR, aSKNA, and EDA using the timing of VM performance as an input. Model parameters were optimized for both datasets (Study 2023 and Study 2024) using the Nelder-Mead method, suitable for non-linear problems. Model performance was assessed using the coefficient of determination (R^2) and the (normalized) Root Mean Square Error (RMSE).

Results The results from Study 2023 and Study 2024 were generally comparable. Yet, Study 2024 exhibited lower aSKNA values and lacked usable EDA data. The model demonstrated adequate performance metrics on Study 2023, Tertoolen's dataset, with R-squared values and NRMSEs of 0.623 and 0.257 for HR, 0.770 and 0.193 for aSKNA, and 0.587 and 0.041 for EDA. The model performed slightly worse on the newly obtained dataset, Study 2024, with an R-squared value of 0.075 and an NRMSE of 0.379 for HR, but the model achieved an R-squared value of 0.692 and an NRMSE of 0.199 for aSKNA. The HR prediction, in particular, exhibited timing issues.

Conclusion This thesis explored the functioning of autonomic cardiac regulation by developing a simplified model. The sympathetic response to the VM was measured in ten participants by recording ECG and acquiring HR and aSKNA. An additional dataset with six participants, recorded earlier by Tertoolen in 2023, which also included EDA, was utilized. The model predictions showed a useful resemblance to measurements, giving insight into the role of the ANS in cardiac regulation, although further model and parameter optimization is necessary.

Keywords – Autonomic cardiac regulation, Sympathetic Skin Nerve Activity, Valsalva Manoeuvre, Electrocardiogram, Electrodermal Activity, Mathematical modelling

ACKNOWLEDGEMENTS

I would like to thank my supervisor Ying for providing me with this research assignment and giving helpful feedback throughout the process. I want to congratulate you again on the birth of your beautiful daughter - I wish you all the best on your journey together. I appreciate your optimism, perseverance, and realistic perspective.
Runwei, I hope you continue to explore and enjoy the Netherlands and your PhD journey. Thank you for your daily supervision and collaboration.

I would also like to extend my thanks to the rest of my graduation committee: Goos, Frank, and Dirk. Your insightful questions and engagement highlighted the value of this research. The BSS group provided a motivating and enjoyable working environment. Conducting experiments in the Techmed eHealth house was a cool experience. Thank you, Remco, for your partnership in these experiments and for sharing both the struggles and accomplishments of the graduation process.

Additionally, I would like to thank my boyfriend, family, and friends. Bart, you were always there with a listening ear, a hug and a cheer. You are my comfy person with whom I can share everything. Dian, thank you for the countless study sessions, the funny musical songs about my thesis, the shared chocolates, and the sporty study breaks like swimming and running. A special thanks for creating this incredible cover art. Luuk, I appreciate our study sessions together and I think we could be great friends. Joining the DHC Drienerlo hockey association five years ago was one of the best decisions I made. It always felt like home, and even though I am still not a pro(f) at field hockey, I learned a lot and enjoyed every moment. It provided necessary distractions from my studies. To my fellow 'scriptie noobs' of ladies 8, thank you.

I am grateful for my loving family, who have always supported me. Thank you, Tijmen and Yannick, for the occasional study sessions together. Nienke, I appreciate your input on writing and sharing our research experiences. Thank you for being the best sister. Mom and Dad, thank you so much for always, always, being there for me, helping me become the best version of myself and providing valuable criticism.

CONTENTS

ABBREVIATIONS

ANS	Autonomic Nervous System
ARMA	Autoregressive Moving Average
aSKNA	average Skin Sympathetic Nerve Activity
BP	Blood Pressure
BR	Breathing Rate
CDA	Continuous Deconvolution Analysis
CNS	Central Nervous System
ECG	Electrocardiography
EDA	Electrodermal activity
EDL	Electrodermal Level
EDR	Electrodermal Response
ENS	Enteric Nervous System
eSKNA	envelope Sympathetic Skin Nerve Activity
HR	Heart Rate
HRV	Heart Rate Variability
IIR	Infinite Impulse Response
IRF	Impulse Response Function
LTI	Linear Time Invariant
MAP	Mean Arterial Pressure
NRMSE	Normalized Root Mean Square Error
NTS	Nucleus Tractus Solitarii
PNS	Peripheral Nervous System
PSNS	Parasympathetic Nervous System
RMSE	Root Mean Square Error
SC	Skin Conductance
SCL	Skin Conductance Level
SCR	Skin Conductance Response
SKNA	Sympathetic Skin Nerve Activity
SMNA	Sudomotor Nerve Activity
SNS	Sympathetic Nervous System
SSNA	Skin Sympathetic Nerve Activity
VG	Visibility Graph
VM	Valsalva Manoeuvre

1

INTRODUCTION

The average human body possesses more than 7 trillion nerves[2]. This profoundly complex system[3] is an essential part of humans. The ANS controls involuntary processes such as heart rate, digestion, and respiratory rate to maintain homeostasis of among others, blood pressure, within the body. Dysfunctions in the ANS, such as hyperactivity or hypoactivity, can lead to a variety of health issues, including cardiovascular diseases, gastrointestinal disorders, and metabolic imbalances. The ANS is subdivided into the SNS and the Parasympathetic Nervous System (PSNS). The ANS is crucial in cardiac regulation. Modelling the autonomic cardiac regulation adds to the physiological understanding of the cooperation between the cardiovascular system and the ANS in maintaining constant blood pressure as well as keeping the heart rate and blood pressure within physiologically acceptable boundaries. Furthermore, it helps in the early detection of cardiac or autonomic nervous system issues. With a better understanding of how cardiac regulation functions, it becomes easier to detect dysfunctions and their underlying causes. By developing accurate models, different conditions can be simulated and the outcomes of various interventions can be predicted, ultimately improving diagnosis, treatment, and management of ANS-related disorders. Furthermore, such models can facilitate the development of targeted therapies and personalized medicine approaches, contributing to better health outcomes and quality of life for individuals affected by ANS dysfunctions.

This thesis will focus mainly on the SNS as the sympathetic nerve activity can be easily (indirectly) measured via the skin using conventional ECG, called SKNA[4, 5]. The sympathetic nerve activity is intricately linked to individuals' fitness levels and has implications for both cardiac as well as non-cardiac diseases and autonomic dysfunctions[4, 6]. The method to record SKNA is innovative and non-invasive and based on branches of sympathetic nerves within the skin. The activity signal is at ultra-low voltage levels and needs to be sampled at a high sampling rate. Subsequently, the retrieved signal can be processed using a high-pass filter to retrieve the SKNA[7]. For this research, the targeted frequency range is 500 to 1000 Hz. The signal is in the order of a few microvolts, ranging from about -50 to 50 µV.

Understanding the dynamics of the ANS and simulating specific aspects, such as the SKNA, holds significant interest and relevance in physiological modelling. Creating an explainable, physiological and dynamic model of autonomic cardiac regulation, including SKNA simulation, will provide a more comprehensive understanding of the body's regulatory mechanisms under both normal and abnormal conditions. The model's accuracy and correspondence to reality can be evaluated by comparing the model with experimental data. This approach helps detect signs of abnormal autonomic innervation, which may be challenging to observe clinically. Existing cardiovascular models are often too detailed and even focus on the level of individual nerves[8]. The models have simulated the HR, vascular resistance, and the (para)sympathetic tone[9] or thoracic sympathetic nerve activity[8]. However, the aSKNA in combination with HR and EDA has not been simulated before.
The recent development of non-invasive methods to measure the sympathetic tone via ECG, SKNA, has created new opportunities. These methods make it easier and more cost-effective

to evaluate the SNS. Continuous monitoring is possible while maintaining patient comfort and safety. Additionally, they require less specialized knowledge compared to prevalent techniques like microneurography[10]. Furthermore, microneurography is invasive as needles are inserted into individual neuron fibres (the activity measured with this method is called Skin Sympathetic Nerve Activity (SSNA))[11]. Consequently, SKNA can be more widely adopted in both clinical and research settings.

At present, there are several models available which aim to simulate the HR or the ANS. For example, the master thesis of Svendby[12] proposed a mathematical model to simulate HR during cycling and Thoonen et al.[13] predicted HR during several activities, in his master thesis.

Ishbulatov et al. proposed a mathematical model[14] during a (passive) head-up tilt test of the cardiovascular autonomic control. However, the precise mathematics of their model were not disclosed. Some models delved deeper into the baroreflex mechanism, which helps maintain nearly constant blood pressure levels. For example, Rybak et al. proposed a model of a sympatho-respiratory brainstem network[8]. They focused on modelling the effects of the baroreflex on respiratory activity. Doyle et al. proposed a closed-loop model of the baroreflex[15] with first and second-order neurons. In 2006 and 2008 Olufsen et al. published two significant articles employing a baroreflex model for HR regulation during orthostatic stress[16] and postural changes[17]. Sturdy, Ottesen, and Olufsen explored the specifics of modelling the differentiation between A- and C-type baroreceptor firing patterns[18]. Some models focused on estimating subject-specific cardiac parameters and simulating hemodynamics. In 2007, Neal and Bassingthwaighte already estimated subject-specific cardiac output[19] and blood volume during hemorrhage. Additionally, in 2006, Liang and Liu simulated hemodynamic responses to the Valsalva Manoeuvre [20]. In 2010, Hemalatha and Manivannan[21] conducted a similar study, also using a lumped parameter electrical analog model. Lastly, Kana and Holcik[9] provided significant inspiration for this thesis with their simplified mathematical model of cardiovascular control during the Valsalva Manoeuvre as they also quantified the sympathetic tone and made a comparison with Heart Rate Variability (HRV) (a common biomarker of ANS response[22]).

Though comprehensive, the existing models lack the desired level of simplification and the simulation of the aSKNA and EDA. EDA can be integrated as a complementary signal and can be relatively easily measured using wearable devices. Therefore, it is particularly useful to understand its relationship with the ANS. This research aims to bridge this gap by developing a simplified autonomic cardiac regulation model. Additionally, the project aims to compare simulated data, including aSKNA and HR, with recorded data sets, acquired during this research and earlier by Jacomine Tertoolen[1]. Her master thesis 'Evaluation of the Cardiac Tone by Sympathetic Skin Nerve Activity', aimed to estimate cardiac tone using SKNA with the ultimate goal of evaluating stellate ganglion blockades (a medical intervention to reduce Ventricular Arrhythmias). She concluded that the SKNA seems indeed correlated with various parts of the ANS, providing a strong rationale for continuing research in this direction. Therefore, it is also beneficial to develop a model to better understand this correlation. Tertoolen recorded a large data set consisting of a pilot study as well as a validation dataset. These data included SKNA, HR, Breathing Rate (BR), and HRV, and for the pilot study also EDA. Additionally, during this research, experiments were conducted with 10 healthy subjects. During the experiments, the Valsalva Manoeuvre[23] was used as a disturbance of the system which lowers the Blood Pressure (BP) and stimulates the sympathetic nervous system to increase the

BP. In this way, the aSKNA and EDA are expected to transiently increase which can be verified in the model and compared to experimental data. This method was also used in Tertoolen's study to stimulate the sympathetic systems of the subjects.

In this study, to achieve the objectives of creating an autonomic cardiac regulation model and validating simulated features against experimental data, a comprehensive literature review was undertaken to gather background information on the nervous system, particularly focusing on the Sympathetic Nervous System (SNS). The relation between various organs and subsystems was explored, leading to the formulation of a logical feedback system represented by appropriate, approximate, mathematical equations. The model was implemented using MATLAB's `Simulink`[24]. Subsequently, parameter estimation was performed using the Nelder-Mead method, an optimization technique well-suited for nonlinear problems. MATLAB's `fminsearchbnd` function, which finds the local minima of a cost function, was employed to derive the estimated parameters. The ultimate validation of the model's efficacy involved a comparison with real data, referring to Tertoolen's recorded dataset from 2023 and the experimental data acquired during this research. The model's performance was quantified by the coefficient of determination, the R-squared, the RMSE and the Normalized Root Mean Square Error (NRMSE), normalized with respect to the range of the measured data. The hypothesis was that a well-simplified cardiac regulation model could be created which further enhances understanding of the ANS and its role in cardiac function. Besides, simulated features related to ANS performance were expected to show a satisfactory resemblance to experimentally obtained features.

This thesis follows the subsequent structure: chapter 2 provides background information and an overview of recent studies regarding SKNA, chapter 3 describes the methodology of data acquisition, data processing and the development of the autonomic cardiac regulation model. Chapter 4 presents the results. In chapter 5 an elaborate discussion on these results can be found, and final conclusions are given in chapter 6. Appendix A contains the code, subject specifics, and individual results.

2

BACKGROUND

This chapter provides background information on the division of the nervous system, signals related to autonomic nervous activity, the functionality of the baroreflex mechanism, and tests that stimulate the baroreflex and ANS activity. Additionally, an overview of the state of the art in SKNA and EDA is presented.

2.1 THE NERVOUS SYSTEM

The nervous system receives signals from different body parts about external changes and responds to them by sending new signals back. The nervous system (see fig. 1) consists of the Central Nervous System (CNS) and Peripheral Nervous System (PNS), respectively, the brain and spinal cord, and the nerves which connect the spinal cord to the rest of the body. The ANS[25] is part of the peripheral nervous system and controls involuntary processes, e.g. digestion, heart rate, and breathing rate. The ANS is then subdivided into the SNS, the PSNS, and the Enteric Nervous System (ENS). The SNS activates the body, also called the "fight-or-flight-response". Sympathetic activation effects include increasing heart rate and cardiac output. At the same time, the PSNS stimulates the activities which occur when the body is at rest (these include digestion, lacrimation (crying), and sexual arousal). These activities are called "rest and digest" processes. The parasympathetic tone slows down the heart rate. The ENS, on the other hand, encompasses reflex pathways which control the muscles of the digestive system and its secretion or absorption and blood flow. It is sometimes even categorized as an independent system and has many neurons structured like a mesh. Understanding the interaction between the SNS and PSNS is important to accurately model autonomic cardiac regulation.

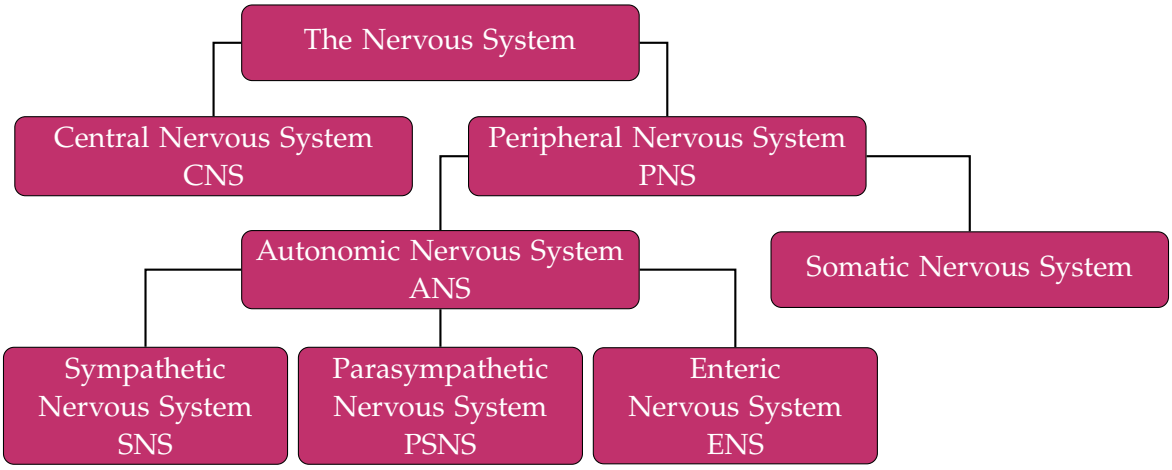

Figure 1: Schematic overview of subdivisions of the nervous system.

2.2 SIGNALS RELATED TO ACTIVITY OF THE ANS

Autonomic activity is reflected by many body signals that relate to involuntary processes. The classic (psychophysiological) lie-detector, or polygraph [26, 27] is an example of a device which combines multiple signals to tell whether someone is dishonest. Deception[28] requires more effort and thus causes a higher or different cognitive and emotional response which is often described as fear or arousal. These emotions cause an elevated autonomic response. In 1921 the first polygraph was produced by John Larson[27]. It measured respiration rate, blood pressure, and heart rate to detect dishonesty. Nowadays, many signals are used, among others BP, BR, electrodermal Skin Conductance (SC), body temperature, HR, HRV. Autonomic activity is also related to Carbon Dioxide concentration (this was investigated by Braune et al.[29], where sympathetic activity was stimulated by applying hypercapnia conditions, and Jordan et al.[30] suggested that sympathetic activity also influences the cerebral vasculature and thus indirectly the CO_2 levels). Moreover, ANS activity influences cardiac output, baroreceptor response, pupil[31] dilation, and the recently discovered aSKNA.

2.3 BAROREFLEX

The autonomic cardiac regulation is heavily dependent on the baroreflex[32]. The baroreflex aims to maintain homeostasis of the arterial bloodpressure and is activated when a change in blood pressure occurs. The baroreceptors are located in the aortic arch and the carotid sinus, where they sense a change in arterial pressure due to the deformation of the viscoelastic wall of the arteries. Subsequently, the receptors will react to this mechanotransduction by adjusting the afferent firing rate accordingly. This information, the firing rate, is sent to the Nucleus Tractus Solitarii (NTS) located in the medulla oblongata of the brainstem. The NTS contains many sensory nuclei. This stimulates the ANS and the sympathetic and parasympathetic tones are produced. Via the vagal nerve, the parasympathetic tone is delivered to the heart, changing its contractility and heart rate. The sympathetic outflow, on the other hand, is transmitted by numerous neurons. The chemicals acetylcholine and noradrenaline are largely responsible for heart rate regulation. Respectively, the parasympathetic system manages the acetylcholine concentrations, and the sympathetic system the noradrenaline concentrations. Due to complexity, the sympathetic system responds slower than the parasympathetic system. Moreover, in case of elevated blood pressure, parasympathetic activity inhibits sympathetic activity. This provokes a decrease in heart rate leading to the desired blood pressure. In summary, the baroreceptors sense changes in blood pressure, transfer this information to the ANS, modulate the heart rate and consequently regulate the blood pressure.

2.4 AUTONOMIC FUNCTION TESTS

Autonomic function tests[34, 35] can be used to trigger the baroreflex and autonomic nerve activity. Examples of such cardiovascular reflex tests consist of the earlier mentioned Valsalva Manoeuvre, but also deep breathing, isometric handgrip test, cold water pressor test, mental arithmetic, head-up tilt test, and orthostatic test. With the deep breathing technique, the difference in heart rate (respiratory arrhythmia) is evaluated, which declines with age. During hand gripping (with the use of a dynamometer) a rise in blood pressure is observed. This increase in blood pressure is again an indicator of autonomic function. Moreover, the cold water pressor test stimulates the subject by using cold water as the name indicates. The subject submerges their hand in a bowl of ice water for a short time (ca. 2 min) which drives the heart rate and

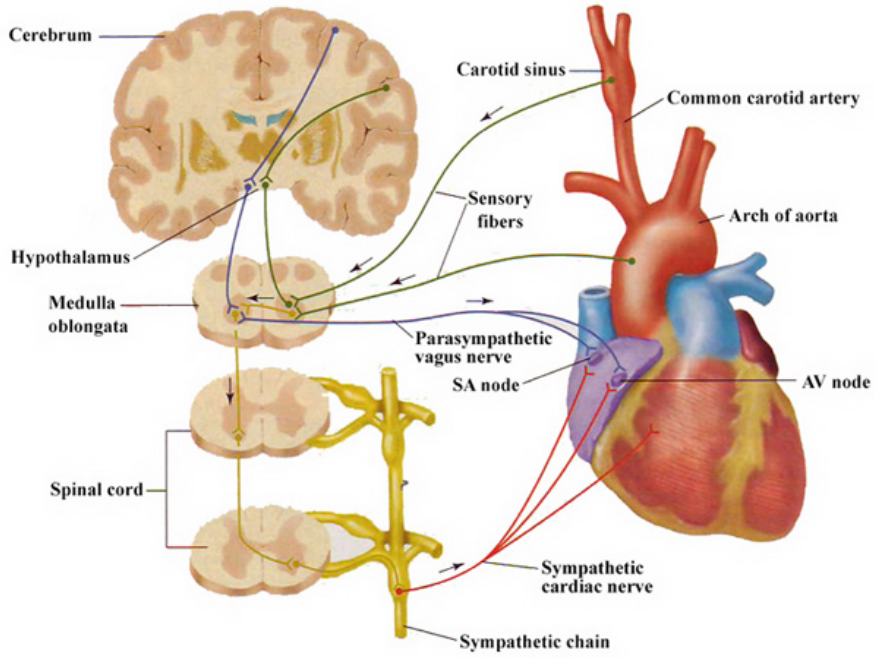

Figure 2: Schematic display illustrating the key anatomical structures involved in the baroreflex[33].

blood pressure up. By providing several small mathematical problems, such as subtractions and additions, the subject is imposed with a mental stressor which activates the sympathetic system. Both the head-up tilt test and orthostatic test are based on moving the body (from a supine or sitting position into a standing position), where the first method is passive and the latter active. The movement ensures a blood flow rush towards the lower limbs and thus a drop in blood pressure. Lastly, pharmacological stimulation, e.g. phenylephrine, can be used to evaluate the sensitivity of the baroreceptors.

The autonomic function test utilized in Tertoolen's study, as well as in this research, involves the VM in conjunction with postural changes (supine-to-sit and sit-to-stand). The VM is a breathing technique in which the subject is asked to inhale deeply and exhale against a closed airway. Subsequently, the intrathoracic pressure increases, the Mean Arterial Pressure (MAP) drops and in turn activates the sympathetic nervous system to ensure that blood pressure increases to the desired level. In fig. 3, the four phases associated with the VM[36] (in a healthy individual) are shown. During phases 1 and 2 the intrathoracic pressure is applied and sustained.

Phase 1: At the onset of the VM the rise in intrathoracic pressure compresses the pulmonary vessels, pushing blood into the left ventricle of the heart. This temporarily increases stroke volume and MAP. The baroreceptor reflex reacts to the increased MAP by briefly lowering the heart rate.

Phase 2: The sustained high intrathoracic pressure then inhibits venous return to the heart. This reduces stroke volume causing a decline in MAP. The baroreceptors facilitate an increase in heart rate, bringing MAP back to near-normal levels.

Phase 3: After, in this case, 10 s, releasing the intrathoracic pressure allows venous return to the intrathoracic vessels. During the experiments of Tertoolen and the experiments performed for this study, subjects were instructed to hold the intrathoracic pressure for 15 s. After this the stroke volume decreases and the MAP drops further leading to an additional reflexive rise in heart rate.

Phase 4: The left heart chamber refills as usual whereafter the MAP rises. With a still elevated heart rate, the MAP overshoots. The baroreflex quickly adjusts this resulting in reflex bradycardia. Finally, the MAP and heart rate return to baseline.

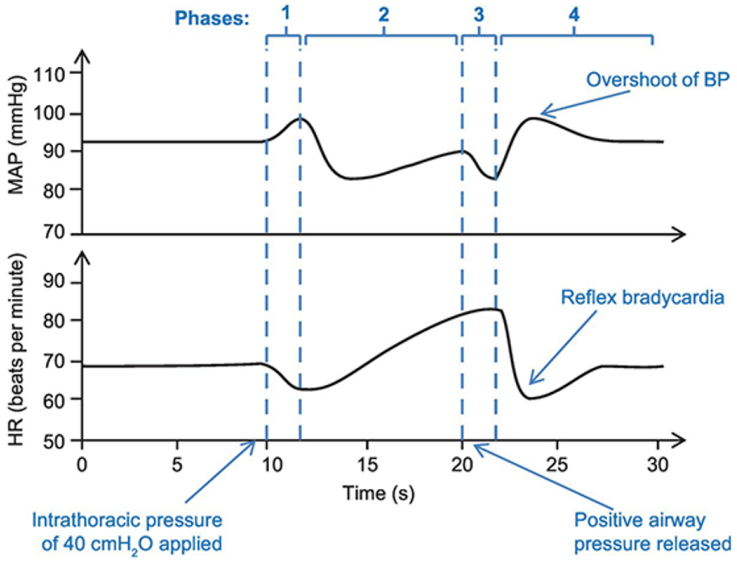

Figure 3: MAP and heart rate during the Valsalva Manoeuvre, taken from[36].

2.5 SKIN SYMPATHETIC NERVE ACTIVITY

In recent years a growing interest has been shown in the various functionalities of SKNA. The non-invasive method for SNA assessment has been proven useful in clinical studies in various fields (e.g. [6, 37, 38]). In table 1 an overview can be found of such studies. Baseline aSKNA values show dispersion and are between 0.77 µV and 2.5 µV. Numerous studies show correlation between (a)SKNA and different diseases[4] and fitness[6]. The functioning of the ANS is complicated and although sympathetic activity is related to many diseases it cannot be used as a marker for a specific condition. Moreover, given the wide variability of reported values, an isolated aSKNA value may not be particularly informative and should always be interpreted within a broader context. Some features derived from SKNA signals that are commonly used are the mean aSKNA, number of bursts, inter-burst interval, burst duration and area, and burst amplitude. Previously, HRV analysis was used to assess autonomic activity[39]. However, this method is limited by its focus on the sinoatrial node and its inability to provide real-time information. In contrast, SKNA provides a better reflection of overall and current sympathetic activity. Cai et al. provided a new, quantitative, method for ANS assessment by employing Visibility Graph (VG)[40] on envelope Sympathetic Skin Nerve Activity (eSKNA). This nonlinear dynamics analysis method effectively evaluated the ANS from a network aspect. VG features (based on SKNA) were found to be superior over HRV features in distinguishing cerebral hemorrhage patients from control group patients. Li and Zheng published a review on current cardiac sympathetic activity assessment methods[41]. They noted that while SKNA can non-invasively record cardiac sympathetic nerve activity, the method has certain limitations. Specifically, movement artefacts from patients significantly affect the quality of the recorded signals. Additionally, SKNA lacks established reliable reference values. Furthermore, it is worth noting that Xing et al.[42] proposed a modification at system level by combining an analogue front-end chip with a low-noise first-stage amplifier, an adaptive PLI filter and clipping of outliers. This reduced system noise and motion artefacts.

Overall, SKNA is regarded as a valuable and respected method for assessing SNA, which has proven useful in evaluating people's health. Therefore, modelling autonomic regulation and its role in cardiovascular health, along with simulating aSKNA, can provide valuable insights into underlying mechanisms. A simplified and explainable model can particularly enhance the understanding and application of these findings. The processed aSKNA contains fewer artefacts than the SKNA and is considered to more accurately capture the essence of the SNA. Consequently, it is more logical and feasible to model. Additionally, the field would benefit from implementing more uniform standardization procedures for SKNA processing.

Table 1: Summary of recent studies regarding SKNA and associated parameters. Largely based on Tertoolen's literature study[1] with addition of studies conducted since then and up to the present.

Study population	n	Sex (male %)	Age (yr)	BMI (kg/m²)	aSKNA (μV)	Device	fs (kHz)	Reference
Healthy subjects	8	1 (13)	41 ± 11	32.4 ± 5.1	0.89 ± 0.17	BM	10	He, 2020[38]
	12	5 (42)	31.7 ± 7.4	n/a	1.52 ± 0.71	PLS	10	Chen, 2021[43]
	165	97 (59)	47.97 ± 13.59	23.48 ± 3.15	0.77 ± 0.22	BM	10	Huang, 2022[44]
	14	0 (0)	31 ± 6	n/a	.98 ± 0.06	FI80		Lee, 2022[45]
	19	0 (0)	30 ± 6	n/a	1.17 ± 0.31	F180	1	Hwang, 2022[46]
	6	3 (50)	25 ± 2.5	22.9 ± 3.6	0.71 ± 0.21	BM	9.6	Tertoolen, 2023[1]
	47	20 (42)	26.5 ± 11.4	24.3 ± 3.9	0.77 ± 0.21	BM	9.6	Tertoolen, 2023[1]
	29	4 (13.8)	53.48 ± 9.41	23.78 ± 3.66	0.81 ± 0.24			Chen, 2023[47]
	72	44 (61.1)	57.76 ± 8.74	n/a	1.12 ± 0.35	HF ECG	4	Wang, 2023[48]
	9	5 (55.6)	20-42	n/a	4.05 ± 4.09[1]	Bio Amp	10	Baghestani, 2023[49]
	16	8 (50)	20-57	n/a	0.26 ± 0.13	Bio Amp	10	Baghestani, 2024[49]
Arrhythmias								
Paroxysmal AT	11	4 (36)	66 ± 10	n/a	1.07 ± 0.10	BM	10	Uradu, 2017[50]
VA during unsedated ICD implant	39	35 (50)	66.1 ± 10.2	32.6 ± 5.6	1.41 ± 0.53	BM	10	Zhang, 2019[51]
VA during sedated ICD implant	11	8 (72.7)	58.5 ± 16.2	31.3 ± 5.5	0.83 ± 0.22	BM	10	Zhang, 2019[51]
ICD for primary prevention	15	9 (60)	62.7 ± 16.7	27.4 ± 5.1	0.98 ± 0.41	BM	10	Zhang, 2019[51]
Persistent AF	12	6 (50)	73 (60.5-80)	32.2 (27.4-40.1)	1.09 [0.91-1.33]	BM	10	Kusayama, 2019[52]
Paroxysmal AF	8	4 (50)	66 (59-77)	31.4 [25.5-51.0]	1.12 [1.02-1.30]	BM	10	Kusayama, 2019[52]
LQTS undergoing LCSD	17	8 (47)	21 ± 9	27.51 ± 8.74	1.36 ± 0.67	BM	10	Han, 2020[53]
Proximal SVT	16	6 (38)	44 ± 16	n/a		BM	10	Han, 2020[53]
Electrical storm	1	6 (60)	52.7 ± 12.4	n/a	0.89 ± 0.22	PLS	10	Chen, 2021[43]
TTM at 36 °C post-cardiac arrest	6	5 (83)	52.2 ± 18.8	28.37 ± 4.91	0.90 ± 0.20	BM	10	Kutkut, 2021[37]
TTM at 33 °C post-cardiac arrest	23	16 (70)	51.5 ± 19.3	31.22 ± 9.78	0.76 ± 0.13	BM	10	Kutkut, 2021[37]
Paroxysmal AF	7	3 (43)	57 ± 14	n/a	1.22 ± 0.35	F180	1	Hwang, 2022[46]
Paroxysmal AF	37	34 (92)	58.9 ± 9.0		538.2 [432.9-663.9][2]	MP36	2	Sung, 2022[54]
Coronary Artery Disease								
CAD undergoing CABG	11	7 (64)	60 ± 13	31.1 ± 6.7	2.5 [1.9-3.1]	PLS	10	Shen, 2017[55]
AMI	20	20 (100)	52.8 ± 13.5	27.2 ± 4.2	1.024 [0.852-1.399]	BM	10	Liu, 2021[56]

1 Note that here SKNA is reported instead of aSKNA.
2 See footnote 1.

Study population	n	Sex (male %)	Age (yr)	BMI (kg/m²)	aSKNA (µV)	Device	fs (kHz)	Reference
AMI	20	20 (100)	51.9 ± 14.5	23.6 ± 2.9	0.680 [0.617-0.728]	BM	10	Liu, 2021[56]
CAD	8	5 (62.5)	67.3 ± 9.7	n/a	1.17 ± 0.20	PLS	10	Chen, 2021[43]
ACS	128	110 (86)	57.87 ± 11.72	25.98 ± 4.01	1.05 ± 0.35	BM	10	Huang, 2022[44]
Heart failure								
HFrEF and indication for CRT	36	30 (83.3)	69.1 ± 12.3	30.1 ± 6.2	1.52 ± 0.65	BM	10	Xiao, 2020[57]
LVEF < 35 %					1.58 ± 0.63	BM	10	Xiao, 2020[57]
LVEF > 35 %					0.88 ± 0.36	BM	10	Xiao, 2020[57]
HFrEF and indication for ICD	10	7 (70)	61.7 ± 19.9	27.8 ± 6.0	0.97 ± 0.49	BM	10	Xiao, 2020[57]
Dysautonomia								
NCS, without syncope	36	13 (33)	42.2 ± 15.5	n/a	1.38 ± 0.38	BM	10	Kumar, 2020[58]
NCS, with syncope	14	3 (22)	33 ± 19.1	n/a	1.42 ± 0.52	BM	10	Kumar, 2020[58]
NCS, without syncope	25	8 (32)	42.2 ± 17	n/a	1.02 ± 0.29	BM	10	Huang, 2021[59]
NCS, with syncope	16	4 (25)	46.6 ± 16.1	n/a	1.21 ± 0.30	BM	10	Huang, 2021[59]
OI	16	2 (13)	35 ± 10	n/a	0.99 ± 0.07	F180		Lee, 2022[45]
OI	18	1 (6)	37 ± 11	n/a	1.04 ± 0.11	F180	1	Hwang, 2022[46]
OI, without drugs	17	2 (12)	39 ± 12	n/a	1.03 ± 0.13	F180		Lee, 2022[45]
Neurological disorder								
Drug resistant epilepsy with VNS	6	2 (33)	40 ± 11	n/a	1.06 [0.93-1.18]	BM	10	Yuan, 2017[60]
Drug resistant epilepsy without VNS	20	7 (35)	37 ± 8	n/a	1.38 [1.01-1.75]	BM	10	Yuan, 2017[60]
Other								
OSA	18	6 (33)	50 ± 17	37.5 ± 12.1	0.96 ± 0.36	BM	10	He, 2020[38]
Esophageal squamous cell carcinoma	39	36 (92)	59.15 ± 6.56	23.28 ± 3.28	0.77 ± 0.03	BM	10	Tang, 2022[61]
Undergoing HD with an IDWG > 3 kg	25	18 (72)	51.0 [44.5-60.5]	24.1 ± 3.6	1.11 ± 0.29	CMD	4	Zhang, 2022[62]
Undergoing HD with an IDWG < 3 kg	51	30 (59)	66.0 [50.0-71.0]	22.6 ± 4.0	1.18 ± 0.42	CMD	4	Zhang, 2022[62]
OAB	23	1 (4.3)	54.43 ± 10.09	23.85 ± 3.86	1.08 ± 0.37			Chen, 2023[47]
OAB, post-treatment	23	1 (4.3)	54.43 ± 10.09	23.85 ± 3.86	0.94 ± 0.33			Chen, 2023[47]
OAB with DO	10	1 (10)	56.70 ± 9.63	24.70 ± 4.80	1.24 ± 0.42			Chen, 2023[47]
OAB without DO	13	0 (0)	52.69 ± 10.21	23.19 ± 2.96	0.95 ± 0.27			Chen, 2023[47]
ICH	77	52 (67.5)	60.52 ± 16.38	n/a	0.87 ± 0.34	HF ECG	4	Wang, 2023[48]
POTS	79	7 (8.9)	36 ± 11	25		Faros 180 ECG	1	Liu, 2023[63]

Data are means ± SD or numbers (proportions). ACS = acute coronary syndrome, AF = atrial fibrillation, AMI = acute myocardial infarction, AT = atrial tachycardia, BM = Biomonitor, CABG = coronary artery bypass graft, CAD = coronary artery disease, CMD = custom-made device, CRT = cardiac resynchronization therapy, fs = sampling frequency, F180 = Faros 180 ECG monitor, HD = hemodialysis, HFrEF = Heart failure with reduced ejection fraction, ICD = implantable cardioverter-defibrillator, IDWG = interdialytic weight gain, LCSD = left cardiac sympathetic denervation, LQTS = long QT syndrome, LVEF = left ventricle ejection fraction, MP36 = MP36 system (BIOPAC Systems), NCS = neurocardiogenic syncope, OI = orthostatic intolerance, OSA = obstructive sleep apnea, PLS = Powerlab System, SVT = supraventriclar tachycardia, TTM = targeted temperature management, VA = ventricular arrhythmia, VNS = vagal nerve stimulator, OAB = overactive bladder, DO = detrusor overactivity, ICH = intracerebral hemorrhage, POTS = postural orthostatic tachycardia syndrome.

2.6 ELECTRODERMAL ACTIVITY

EDA[64] is the electrical activity measured on the skin. The conductivity of the skin varies mainly due to sweat secretion. This was first discovered[65] in 1878 by the Swiss Hermann and Luchsinger. Sweat excretes from the sweat glands, which lie in the dermis, below the epidermis. Within the epidermis, the stratum corneum is the outermost layer composed of dead skin cells. This barrier can be compared to a resistor.

There are two types of sweat glands, namely, eccrine and apocrine. Apocrine sweat glands are rarer and can be found in specific locations such as armpits, areola and perineum. The eccrine ones on the other hand constitute the majority of sweat glands in humans. They include sweat ducts and secretory coils. The ducts spiral through the cornified layer ending up as sweat pores on the skin. Clearly, the main purpose of sweat secretion is to provide thermoregulation to maintain homeostasis of the body temperature. The evaporation of sweat expends energy and leads to the cooling of the skin and consequently a decrease in body temperature. However, perspiration is not only related to thermal sweating but also to emotional sweating. Two other uses involve skin responses during the preparation of specific motor actions and reticular formation in the brainstem through general arousal. Sudor related to sympathetic activity is predominantly present on palmar and plantar sites.

Sympathetic nerves innervate the sweat glands and, as sympathetic activity activates the body, EDA is linked to psychological and physiological arousal. This was proven during microneurography studies[66]. Sudomotor neurons are part of the autonomic nervous system. Each sudomotor is specialized to control several sweat glands and each sweat gland is controlled by multiple sudomotor neurons.

EDA can be recorded either exosomatically or endosomatically[65]. The first applies direct or alternating current to the skin and records the change in skin conductance or resistance. The latter, however, records electric potential differences within the skin, without external current. The endosomatic method results in monophasic, biphasic, or triphasic skin potential responses, which are difficult to analyze and understand. Therefore, the exosomatic method is preferred.

The electrical system consists of the skin and its sweat glands, and a measurement system. Here, biological mechanisms that drive the electrical responses can be seen as the voltage source and the stratum corneum serves as a variable resistor according to its hydration degree. The deeper layers of the skin have fixed but relatively low resistance. Lastly, the sweat gland ducts act as shortcuts that allow electrical current to flow more easily through the skin.

Electrodermal activity consists of a tonic component and a phasic component[65]. These are called the Skin Conductance Level (SCL) and Skin Conductance Response (SCR) when measured via the exosomatic method. Otherwise, they are referred to as the Electrodermal Level (EDL) and Electrodermal Response (EDR). The SCL is independent of any applied stimuli. It can be influenced by factors like the (skin or ambient) temperature. The phasic response is known to be linked with sudomotor nerve activity triggered by physiological stimuli.

EDA analysis

In the past, various mathematical methods have been developed to analyze recorded EDA and model the components of interest, the phasic and tonic components. These methods aim to decompose the phasic signal into individual SCRs linked to each stimulus and model how sympathetic activity prompts these SCRs. Earlier methods often required visual inspection to resolve the overlap issue, where individual SCRs caused by different separate stimuli overlap. However, this led to subjectivity in analysis.

Barry et al.[67] used graphical tools to improve the baseline by subtracting each SCR from the preceding SCR. For this Lim et al.[68] used a response function with 4-8 parameters optimized for each SCR, allowing for variations in individual SCR shapes. This method also needed visual inspection to choose the best model.

Alexander et al.[69] introduced the first Linear Time Invariant (LTI) model for EDA analysis. Due to the description of the peripheral system as an LTI system more automation in analysis was possible. [69]'s model interprets skin conductance as the convolution of bursts of sudomotor nerve activity with a fixed Impulse Response Function (IRF), aiming to estimate sympathetic nervous system activity from observed SC data. Benedek and Kaernbach criticized (part of) Alexander et al.'s model and introduced two alternative LTI approaches: nonnegative deconvolution [71] and Continuous Deconvolution Analysis (CDA)[70]. In these models, the LTI assumption was refined to include the variability in SCR shape. They partition SMNA into components describing phasic activity and EDA variations, assuming a pharmacokinetic model of sweat diffusion dynamics. Both models employ a biexponential IRF known as the Bateman function. While observation noise is acknowledged in the above-mentioned methods, it was not explicitly modelled. Instead, a noisy SMNA was estimated and the phasic component was retrieved by low-pass filtering and applying a heuristic peak detection.

In 2014, Bach introduced the SCRalyze toolbox[72] for analyzing evoked SCRs. The software package includes multiple models based on an LTI system assumption. Both Alexander et al. and Bach use an IRF optimized on big datasets. SCRalyze employs optimization techniques to estimate the input signal, SMNA, or parameters that best fit the observed SC data. Additionally, these models include a noise term to address potential deviations from time invariance assumptions.

Shortly after, Greco et al. introduced a method for the decomposition[74] of SC into smooth tonic and sparse phasic components. They achieve this by solving a convex optimization problem and incorporating physiological constraints and regularization terms. For example, a nonnegative constraint was imposed because of the inherently positive nature of SMNA. In 2016 they proposed a new approach to estimate ANS activity from EDA again using convex optimization[73]. The model is based on Bayesian statistics and represents SC as three components: a steady tonic component, obtained through the convolution of an IRF, a sparse nonnegative SMNA phasic driver, and additional noise. The IRF is represented using an Autoregressive Moving Average (ARMA) model to create an Infinite Impulse Response (IIR) function. This model provides more accuracy than a FIR approach by avoiding the need to truncate the IRF. Additionally, it achieves higher computational efficiency due to a concise system representation.

In summary, this chapter highlighted the roles of the sympathetic and parasympathetic branches of the ANS in active and relaxing involuntary processes. Together with the baroreceptors, they maintain homeostatic blood pressure by increasing and decreasing heart rate, respectively. Autonomic function tests such as the VM effectively trigger autonomous nervous responses. The manoeuvre entails four characteristic phases. During the first two phases, subjects exhale against a closed airway, thereby maintaining high intrathoracic pressure, leading to an increase in HR and SNA. Afterwards, the air is released and the MAP and HR are restored. The chapter also underscored the significance of SKNA and the added value of EDA in assessing SNA, autonomic cardiac regulation, and overall health. Finally, compelling reasons were given to model this complex system.

3

METHODS

The following chapter describes the methods used for retrieving and analyzing the experimental data. Furthermore, a model is presented that describes the basics of autonomic cardiac regulation.

3.1 MATERIALS

This section describes the study designs of the experimentally obtained data by Tertoolen and this research.

Study Design Tertoolen: Study 2023

An explorative study was performed by Jacomine Tertoolen[1] between 2022 and 2023, providing an elaborate dataset, referred to as 'Study 2023'. A pilot study was executed with six healthy adult subjects. Their characteristics can be found in table 2.

Table 2: Subject characteristics for Tertoolen's pilot [1], Study 2023. The data are means ± standard deviation or numbers (with proportions in % in brackets). BMI is the Body Mass Index and BSA is the Body Surface Area.

	Pilot dataset ($n = 6$)
Age (yr)	25.0 ± 2.8
Sex (male)	3 (50%)
Length (m)	1.75 ± 0.11
Weight (kg)	69.3 ± 8.8
BMI (kg/m^2)	22.9 ± 3.9
BSA (m^2)	1.83 ± 0.12

The following equipment was used:

- the Biomonitor ME6000 (Mega Electronics Ltd., Kuopio, Finland[75]) to record ECG with a sampling frequency of 4800 Hz,
- 12 Ag/AgCl electrodes (3M, Minnesota, USA)
- the Shimmer3 GSR+ (Shimmer, Dublin, Ireland[76]) to record EDA with a sampling frequency of 64 Hz.

Four leads were calculated from twelve electrodes connected to the Biomonitor that were applied to the subjects as shown in fig. 4. The Shimmer3 GSR+ was put on the index and middle finger on the right hand of the subject. The protocol can be seen in table 3.

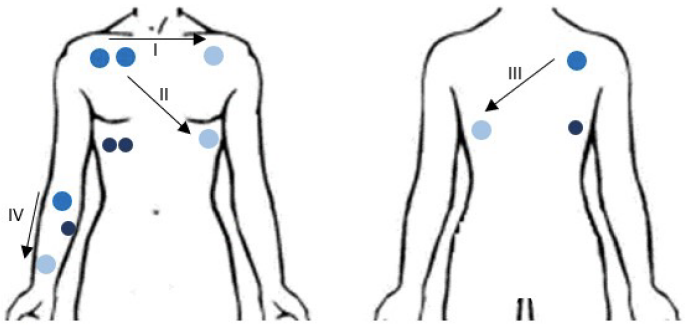

Figure 4: Set-up of the electrodes and leads during the pilot experiment of Tertoolen[1], Study 2023. Roman numbers indicate leads, where light blue indicates a positive electrode and darker blue is a negative electrode. The darkest blue dots are the grounds. Leads I and II are in the manner of Einthoven's triangle[77].

Table 3: Protocol for Study 2023, Tertoolen's pilot[1]. The durations are minima that could have been deviated from.

Phase	1	2	3	4	5	6	7
Mode	Lying			Sitting			Standing
Duration (s)	300	15	20	105	15	20	105
Activity	VM1			VM2			

Study Design 2024

Next to Tertoolen's data set, an additional experiment was conducted in the eHealth House at the University of Twente, referred to as 'Study 2024'. The Ethics Committee Computer and Information Science of the University of Twente approved the study (reference number 230728). Ten healthy subjects were recruited for this study of which 70% male. The inclusion criteria were as follows: participants had to be between 18 and 60, have a Body Mass Index (BMI) lower than 40 kg/m², be free of cardiovascular diseases, respiratory diseases, metabolic disorders, and not being pregnant. All subjects signed a consent form to participate in the study and agreed to the use of their anonymized data for scientific research. Subject characteristics can be seen in table 4, while individual characteristics per subject can be seen in appendix A table 9.

Table 4: Subject characteristics for Study 2024.

	Experiment 2024 (n = 10)
Age (yr)	26.8 ± 8.1
Sex (male)	7 (70%)
Length (m)	1.78 ± 0.07
Weight (kg)	73.0 ± 11.5
BMI (kg/m²)	23.0 ± 3.2

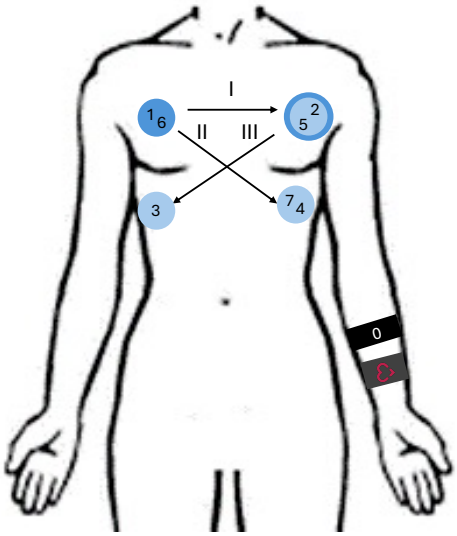

Figure 5: Set-up of the sensor distribution for the experiment in the eHealth House, Study 2024. The numbers indicate channels and 0 indicates the Patient Ground wristband just above the Empatica E4. Roman numbers indicate leads, where light blue indicates a positive electrode and dark blue is a negative electrode. Electrodes 1, 2, 3, and 4 consisted of smaller patches more suitable to record SKNA, while 5, 6 and 7 are larger electrodes.

The equipment included:

- Smartwatch (Empatica E4, Cambridge, United States of America[78]) to record EDA with a sampling frequency of 4 Hz,
- Sixteen channel Refa Amplifier (TMSi international, Enschede, the Netherlands [79]) able to record with sampling frequencies up to 20 kHz, set to record ECG with a sampling frequency of 2048 Hz, with associated accessories; cables, Patient Ground wristband, USB cable, electrodes etc.

The set-up is schematically shown in fig. 5. The Empatica was used to record electrodermal activity at the wrist and the Refa was used to record and amplify the heart's electrical activity. The protocol was similar to Tertoolen's timeline. It can be found in table 5.

Table 5: Activity timeline for Study 2024.

Phase	1	2	3	4	5	6
Duration (s)	60	30	15	30	15	30
Activity	Lying	Sitting	VM1	Standing	VM2	Standing

3.2 DATA PROCESSING

Figure 6 shows the pipeline used for data analysis in this research. Data analysis was performed using `MATLAB`. After data collection, leads were calculated from the raw ECG data (according to figs. 4 and 5). A lead is the potential difference between the 'positive' and 'negative' electrode. Subsequently, a second-order notch filter was applied at 50 Hz with a 1.43 Hz bandwidth at the -3 dB point to remove powerline noise. The data were bandpass filtered with a second-order Butterworth filter between 0.5 and 40 Hz to retrieve clear ECG, accord-

ing to Ricciardi et al.[80]. These frequencies were chosen to optimize ECG quality. This study used the widely accepted Pan-Tompkins method[81] to detect R-R intervals[82]. The heart rate was computed from these intervals. Subsequently, a sliding window averaging method was applied with a window length of 10 samples and a 5-sample overlap. The data were then resampled to 1 Hz using interpolation to match the frequency of the aSKNA signal.

The notch-filtered data were also band-pass filtered between 500 and 1000 Hz using a fifth-order Butterworth filter to obtain the SKNA. Next, the SKNA data were processed by taking the absolute values and then using a leaky integrator over a 100 ms window, as commonly used[6, 10, 49], yielding the iSKNA. Integration smoothened the SKNA signal, highlighting changes in sympathetic activity. The iSKNA was then averaged over a one-second window to obtain the aSKNA. This ensures further smoothing of the signal. A Gaussian Mixture Model (GMM) was used on the aSKNA data to identify significant events in the experiment. This separated baseline activity from peaks. The threshold was defined as the lowest mean amplitude (of the two Gaussian distributions) with three times the associated standard deviation. This threshold helped classify timestamps associated with notable events during the experiment (such as postural changes and VMs).

For the analysis of the acquired EDA data, Greco et al.'s cvxEDA[73] approach was used. This method models skin conductance y as a combination of three components: the phasic component r, the tonic component t and white Gaussian noise ϵ, which accounts for prediction errors, measurement noise, and artefacts.

$$y = r + t + \epsilon \tag{1}$$

Through convex optimization, the model effectively separates the different aspects of EDA signals. The problem to be optimized is formulated by Greco et al. as follows

$$\begin{aligned} &\text{minimize } \frac{1}{2}\| \overbrace{\overbrace{M q}^{r} + \overbrace{B l + C d}^{t}}^{-\epsilon} - y \|_2^2 + \alpha \| \overbrace{A q}^{p} \|_1 + \frac{\gamma}{2}\|l\|_2^2 \\ &\text{subj. to } \; A q \geqslant 0. \end{aligned} \tag{2}$$

Here, the tonic component t comprises cubic B-splines to represent smooth curves and a linear trend to represent the general linear change of the tonic component over time. B is a tall matrix with cubic B-spline basis functions in its columns, l is a vector of spline coefficients, C is an $N \times 2$ matrix with $C_{i,1} = 1$, $C_{i,2} = i/N$, and d is a 2×1 vector with the offset and slope coefficients of the linear trend. The phasic component r is modelled as an IIR function using an ARMA cascade formulated in matrix form, where M is a tridiagonal matrix with $M_{i,i} = M_{i,i-2} = 1$, $M_{i,i-1} = 2$ with $3 \leqslant i \leqslant N$, and q is an auxiliary variable to find p indirectly. The error term ϵ is assumed to consist of an independent identically distributed sequence of zero-average Gaussian random variables with variance σ^2. p is the Sudomotor Nerve Activity (SMNA) with a tridiagonal matrix A with $A_{i,i} = \psi$, $A_{i,i-1} = \theta$, $A_{i,i-2} = \zeta$, where $3 \leqslant i \leqslant N$, and α is a substitution factor for $\sigma^2/\lambda\delta$. ψ, θ and ζ are defined in the context of the transfer function of the ARMA model. δ is the sampling interval and λ is the average number of spikes per unit of time, thus, $\lambda\delta$ represents the expected firing rate per interval. In the last term, γ substitutes σ^2/σ_l^2, where σ_l^2 is the variance of the amplitude at each knot l_i which is assumed to have a normal distribution and be independent and identically distributed. α and γ control the penalty on the phasic and tonic components, respectively. By increasing α a sparser estimate is created, due to the stronger l^1-norm penalization, with stronger suppression of noise-induced

spurious spikes, but simultaneously it leads to more signal distortion. With a smaller α-term the opposite will happen. Larger values of γ lead to a stronger penalization of l and a smoother solution. Equation (2) describes a convex optimization problem, meaning both the objective and the constraint function are convex. Consequently, the global optimum will be found after rewriting the given problem in standard quadratic programming form and solving it.

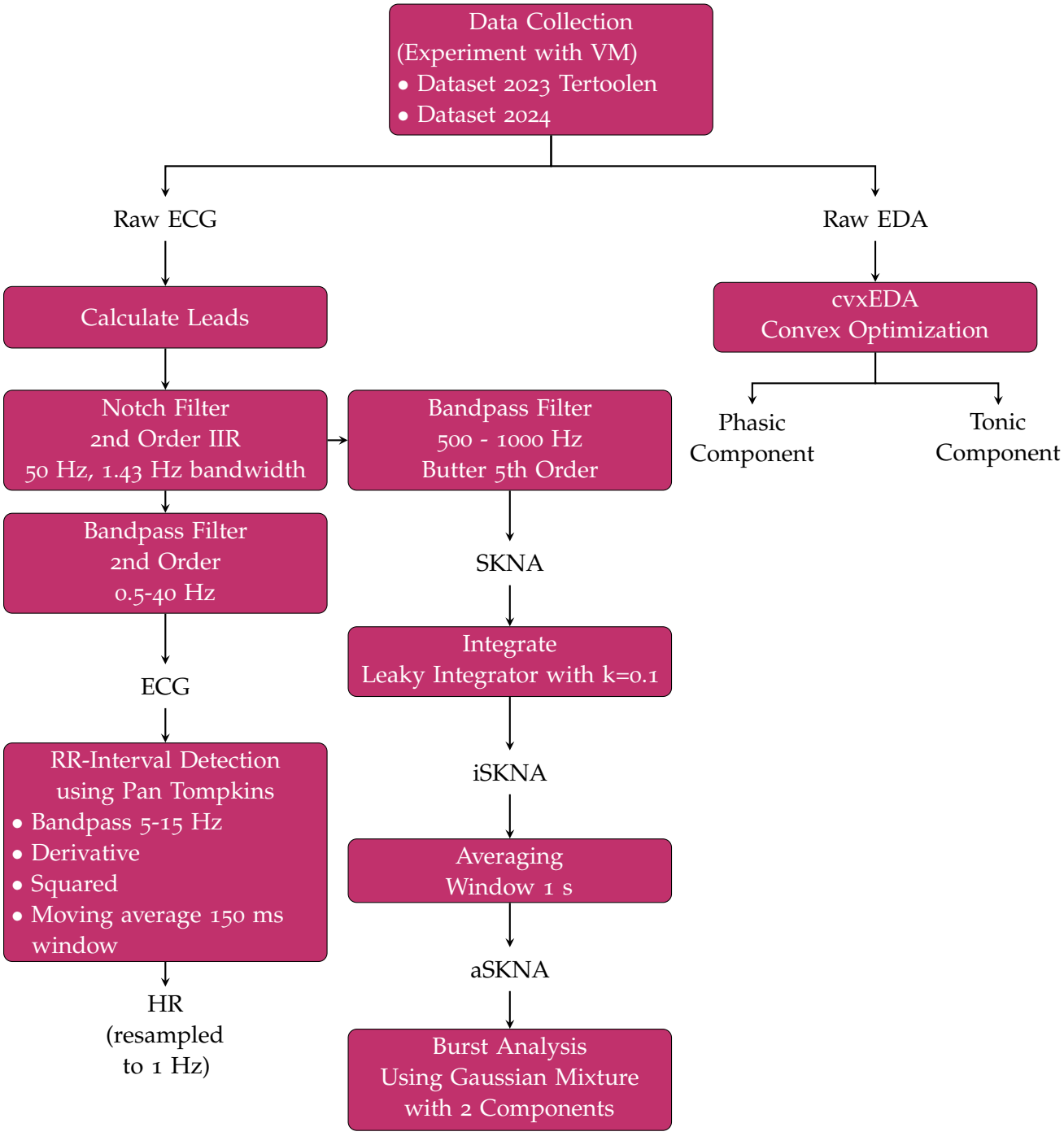

Figure 6: Schematic overview of the signal processing workflow.

3.3 CONCEPTUAL MODEL

The conceptual model consists of several physiological blocks, namely: the baroreceptors, the autonomic nervous system, the pulmonary system, the cardiovascular system and the skin. The cardiovascular system consists of the peripheral system, the heart and the arterial system including large arteries such as the aorta. This conceptual model can be found in fig. 7. The baroreceptors are a sensor which measures the difference between the actual blood pressure (arterial systemic pressure $P_{as}(t)$) and the aspired blood pressure (the mean arterial systemic pressure P_{asmean}). The baroreceptors fire accordingly with a firing rate $n(t)$. The ANS can be seen as the controller as it regulates the heart and peripheral system with the autonomic tone (the parasympathetic $T_{par}(t)$ and sympathetic tone $T_{sym}(t)$ respectively). Besides, the $aSKNA(t)$ was modelled as the sympathetic output. The autonomic tone causes the heart to beat faster or slow down. This leads to a change in Heart Rate $HR(t)$, stroke volume $SV(t)$, and cardiac input $Q_{in}(t)$. At first, when the HR increases the stroke volume will decrease and the cardiac output will initially increase reaching a maximum, whereafter it decreases. Sympathetic activity also influences the peripheral system by increasing the peripheral resistance $PR(t)$. In contrast, the pressure in the venous systemic compartment is approximately constant and is affected by the intrathoracic pressure $P_s(t)$. A regular breathing movement already leads to a difference in intrathoracic pressure transferred by the pulmonary system. Sympathetic nerves innervate the sweat glands present in the skin. This leads to the phasic electrodermal activity signal $y_p(t)$. The tonic activity, known as SCL can be seen as $y_t(t)$. The EDA measured at the surface of the skin, is indicated as $y(t)$.

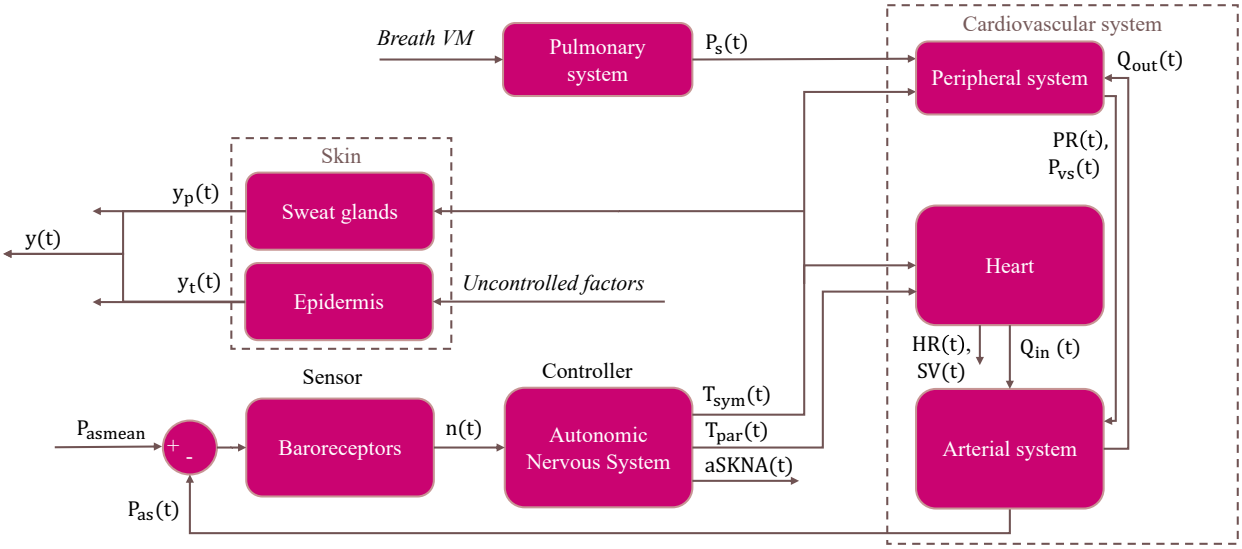

Figure 7: Conceptual model for the autonomic cardiac regulation, where P_{asmean} is the mean arterial systemic pressure, $P_{as}(t)$ is the arterial systemic pressure, $n(t)$ is the firing rate, $T_{sym}(t)$ and $T_{par}(t)$ are the sympathetic and parasympathetic tone and $aSKNA(t)$ the average SKNA, $P_s(t)$ is the intrathoracic pressure, $P_{vs}(t)$ is the venous systemic pressure, and $Q_{in}(t)$ and $Q_{out}(t)$ are the cardiac output and the blood flow through the peripheral system, respectively. $PR(t)$ is the peripheral resistance, $y(t)$ is the EDA, $y_p(t)$ the phasic component and $y_t(t)$ the tonic component. *Breath VM* is the applied disturbance.

3.4 ASSUMPTIONS

Several assumptions were made for the above given conceptual model and the mathematical model that will follow. Here these assumptions are presented and motivated.

1. The model consists of the autonomic nervous system, pulmonary system, cardiovascular system and skin. These capture the key interactions in cardiac regulation. However, it is a simplification, as other factors, such as the influence of hormones, temperature regulation, and metabolic rate, are not taken into account.
2. The modelled subject is assumed to be at rest with constant breathrate and constant intrathoracic pressure $P_s(t)$ until the VM is performed.
3. To describe the arterial systemic pressure $P_{as}(t)$ a first-order differential is used according to Grodins model[83] with an assumed compliance C_{as}.
4. The parasympathetic tone $T_{par}(t)$ is linearly dependent on the baroreceptors' firing rate $n(t)$.
5. The relation of the $aSKNA(t)$ is assumed to be linearly dependent on the sympathetic outflow $T_{sym}(t)$.
6. The sympathetic $T_{sym}(t)$ and parasympathetic $T_{par}(t)$ tones are assumed to be instantly related. This assumption excludes the time delay belonging to the complex sympathetic response.
7. Local and hormone control of arteriolar resistance is negligible. The peripheral resistance $PR(t)$ is dependent on the sympathetic tone $T_{sym}(t)$.
8. A linear effect of the intra-thoracic pressure $P_s(t)$ on the venous systemic pressure $P_{vs}(t)$ is assumed.
9. The arterial walls are assumed to be elastic. The firing rate is not equally sensitive to decreases and increases of carotid pressure[32]. A pressure decrease leads to a faster firing rate response $n(t)$.
10. Concerning the EDA, it is assumed that the tonic component $y_t(t)$ is linked to uncontrolled factors[64], these could include thermoregulation, the general arousal aspect of sweating, humidity, emotional state, and individual physiological variability. This is a slowly varying signal dependent on uncontrolled factors. The phasic component $y_p(t)$ of the EDA is related to sympathetic activity. For this reason, the tonic component was not estimated. Instead, the phasic component $y_p(t)$ was estimated and compared to the phasic component $r(t)$ that was based on the measured skin conductance signal $y(t)$.
11. The rise and decay times for SCRs[84] are expected to remain constant during the experiment. Yet, they can vary per person. These are assumed to be Gaussian distributed. Hence, general parameter estimation was performed to create a general model.
12. SCRs are assumed to follow a Gaussian distribution with a mean and variance[84].
13. The sweat ducts are assumed to be empty at $t = 0$[84].
14. Blood pressure $P_{as}(t)$ and heart rate $HR(t)$ are maintained within the physiological range (for mean arterial pressure this is 60 to 110 mmHg [85, 86] and for heart rate this is about 40[87] to 210 bpm[88]). It should be noted that these are age-specific.

3.5 MATHEMATICAL METHOD

In this section, the mathematics of the afore-introduced model will be tackled. Specifically, first, the cardiovascular system will be approximated to produce heart rate, blood pressure and aSKNA signals, and second, the dermal system to simulate the phasic response of the EDA. For an overview of the used parameters, see the Nomenclature at the end of this chapter.

3.5.1 *Cardiac Regulation*

The cardiovascular model is largely based on Kana and Holcik's mathematical model describing the cardiac mechanism during VM[9]. To model the baroreceptors' response to changes in blood pressure the following equation, derived from [9] and [32], was used:

$$\dot{n}(t) = K \cdot (P_{as}(t) - P_{asmean}) \cdot \frac{(M - n(t)) \cdot n(t)}{\left(\frac{M}{2}\right)^2} - \frac{n - N_0}{\tau}. \tag{3}$$

Here, n is the firing rate (Hz) of the baroreceptors bounded by the minimum N_0 and maximum M threshold firing rate (Hz), K is a weighting factor (Hz/mmHgs), P_{as} is the arterial systemic pressure (mmHg), and τ is the time constant (s) related to the response time. For $n(t) = M$, $\dot{n}(t) = 0 - \frac{M - N_0}{\tau}$. At this point, the firing rate is saturated and can only decrease. However, it will quickly rise again if the measured pressure is lower than the desired blood pressure. In case the actual arterial pressure is equal to the aimed pressure ($P_{as} = P_{asmean}$), the firing rate will again be saturated ($\dot{n}(t) = 0 - \frac{M - N_0}{\tau}$) and reach $n = N_0$.
The autonomic nervous system will translate the baroreceptors' firing rates to a sympathetic and parasympathetic tone, T_{sym}, and T_{par} ([]) respectively. The tones are here defined as dimensionless fractions in the range of $0 \leqslant T \leqslant 1$. This is described in eq. (4)[9].

$$\begin{aligned} T_{par}(t) &= \frac{N_0 + n(t)}{M} \\ T_{sym}(t) &= \frac{1 - T_{par}(t)}{1 + \beta \cdot T_{par}(t)} \end{aligned} \tag{4}$$

Here, β is a dampening factor which considers the inhibitory influence of the parasympathetic tone. The delay of the sympathetic activity relative to the parasympathetic activity is not incorporated in this model. The parasympathetic tone is assumed to be translated to the measurable aSKNA with the following equation:

$$aSKNA(t) = aSKNA_0 \left(1 + K_{aSKNA} \cdot T_{sym}(t)\right). \tag{5}$$

Here, the K_{aSKNA} is a scaling factor, $aSKNA_0$ is the baseline average Skin Sympathetic Nerve Activity in µV. Subsequently, the heart responds to the (para)sympathetic activity. This is modelled (as by Kana and Holcik in [9]) by

$$\begin{aligned} HR(t) &= H_0 \cdot (1 - M_p \cdot T_{par}(t) + M_s \cdot T_{sym}(t)) \\ &= H_0 \cdot \left(1 - M_p \cdot T_{par}(t) + M_s \cdot \frac{1 - T_{par}(t)}{1 + \beta \cdot T_{par}(t)}\right). \end{aligned} \tag{6}$$

In eq. (6), HR is the heart rate (in bpm, beats per minute). H_0 refers to the intrinsic heart rate (bpm) when denervated and it is dependent on age. The intrinsic rate takes place when the autonomic activity is inhibited. M_p and M_s are scaling factors for the parasympathetic and

sympathetic response, respectively. With the change in heart rate, the cardiac output[9] to the arteries will change accordingly.

$$\begin{aligned} Q_{in}(t) &= HR(t) \cdot SV(t) \\ &= H_0 \cdot (1 - M_p \cdot T_{par}(t) + M_s \cdot T_{sym}(t)) \cdot SV(t) \\ Q_{out}(t) &= \frac{P_{as}(t) - P_{vs}(t)}{PR(t)} \end{aligned} \tag{7}$$

Q_{in} is the cardiac output (L/min), the blood flow pumped into the arterial system and SV is the stroke volume. Q_{out} is the blood flow (L/min) out of the arterial system into the peripheral system, related to the arterial systemic pressure P_{as} (mmHg), the venous systemic pressure P_{vs} (mmHg) and the peripheral resistance PR (mmHgmin/L). The stroke volume is defined by Kana and Holcik as

$$SV(t) = K_{str} \cdot \frac{P_{vs}(t)}{P_{as}(t)}. \tag{8}$$

Here, K_{str} is a weighting factor (L/b). At the same time, sympathetic activity influences the resistance in the peripheral system[9]:

$$PR(t) = R_1(t) + PR_0 \cdot (1 + K_{PR} \cdot T_{sym}(t)). \tag{9}$$

Here, R_1 is a variable which will be defined later on. The venous systemic pressure is assumed to be constant when there is no disturbance (created by the breath rate).
Finally, the systemic arterial pressure is approximated by

$$\begin{aligned} \dot{P}_{as}(t) &= \frac{Q_{in}(t) - Q_{out}(t)}{60 \cdot C_{as}} \\ &= \frac{H_0 \cdot (1 - M_p \cdot T_{par}(t) + M_s \cdot T_{sym}(t)) \cdot SV(t) - \frac{P_{as}(t) - P_{vs}(t)}{PR(t)}}{60 \cdot C_{as}}. \end{aligned} \tag{10}$$

Where C_{as} is arterial systemic compliance (L/mmHg). The denominator was multiplied by 60 to convert the units of the blood flow Q from [L/min] to [L/s]. This relation was based on Grodins's [83] model of the mechanical part of the cardiovascular system.

Modelling the Valsalva Manoeuvre

The system is disturbed by the performance of the VM. As explained in section 2.4, this procedure consists of four phases.

In the first phase, the intra-thoracic and intra-abdominal pressure will gradually increase by taking a big breath and holding it. This constricts the pulmonary vessels leading to an increase in peripheral resistance, increasing the stroke volume as well as the arterial systemic pressure. The baroreceptor reflex comes into effect by lowering the heart rate. The increase in peripheral resistance is modelled by a Gaussian function R_1 (mmHgmin/L). This function was chosen to simulate the smooth and symmetrical nature of the pressure change.

$$R_1(t) = R_{1amp} \cdot e^{\frac{-(t - dP_{time} - (P_{1dur}/8))^2}{2 \cdot (P_{1dur}/8)^2}} \quad \text{if } t \geqslant 0 \tag{11}$$

R_{1amp} is the amplitude of the resistance (mmHgmin/L) increase during phase 1, dP_{time} is the start time (s) of the VM, and P_{1dur} is the duration (s) of phase 1. The inclusion of P_{1dur}

in the numerator ensures that the increase in resistance begins slightly after the initiation of the VM, rather than instantaneously. The division by 8 prevents the resistance increase from starting too late. In the denominator, the division by 8, prevents the resistance increase from being overly broad.

Meanwhile, the intrathoracic pressure (mmHg) is modelled with a logistic function. The choice for this function was motivated in order to produce an S-shaped curve, ideal for modelling processes that start with a slow increase, accelerate quickly, and then flatten as they reach a maximum. Additionally, the logistic function is mathematically convenient and its parameters can be easily adjusted.

$$P_s(t) = \begin{cases} \frac{Ps_{max} \cdot 10^{-1} \cdot e^{dP_{rate} \cdot t}}{Ps_{max} + 10^{-1} \cdot \left(e^{dP_{rate} \cdot t} + 1\right)} & \text{if } dP_{time} \leqslant t \leqslant dP_{time} + dP_{dur} \\ 0 & \text{if } 0 \leqslant t < dP_{time} \vee t > dP_{time} + dP_{dur} \end{cases} \tag{12}$$

Here, Ps_{max} is the maximum intra-thoracic pressure (mmHg), dP_{rate} is the rate of increase of pressure (1/s) and dP_{dur} is the duration (s) of phase 1 and 2, the forced expiration. In this case, the growing pressure is bounded by the maximum intra-thoracic pressure. The temporary increase in stroke volume is incorporated by an increase in venous pressure

$$P_{vs}(t) = P_{vs0} + K_{vs} \cdot P_s(t), \tag{13}$$

where K_{vs} is a weighting factor (). No additional variable is introduced during phase 2. However, the stroke volume will change. Due to the high intrathoracic pressure, venous return to the heart is reduced and the stroke volume decreases (leading to a drop in arterial pressure). The baroreflex is triggered again. The stroke volume is now formulated as follows:

$$SV(t) = K_{str} \cdot \frac{P_{vs0} - K_{vs} \cdot P_s(t)}{P_{as}(t)} \tag{14}$$

During the third phase, the intrathoracic pressure is released and the venous return restores the intrathoracic vessels. This pressure drop is modelled by a negative Gaussian function P_3 (mmHg) (again, for simplicity and a smooth symmetrical response):

$$P_3(t) = -P_{3amp} \cdot e^{\frac{-\left(t - dP_{time} - dP_{dur} - (P_{3dur}/4)^2\right)}{2 \cdot (P_{3dur}/8)^2}}, \tag{15}$$

where P_{3amp} is the amplitude of pressure (mmHg) drop during phase 3, dP_{dur} is the duration (s) of the forced expiration (phase 1 and 2) and P_{3dur} is the duration (s) of phase 3. The stroke volume has now changed into

$$SV(t) = K_{str} \cdot \frac{P_{vs0} - K_{vs} \cdot P_s(t) + P_3(t)}{P_{as}(t)}. \tag{16}$$

In phase 4 the arterial pressure starts to rise again after the left ventricle is refilled. The heart rate is still quite high and this results in an overshoot in the arterial pressure as well as the

stroke volume. This is rectified by the baroreflex, leading to a reflex bradycardia, after which all return to normal. The stroke volume through all four phases can be summarized as

$$SV(t) = \begin{cases} K_{str} \cdot \frac{P_{vs0} + K_{vs} \cdot P_s(t)}{P_{as}(t)} \\ \quad \text{if } 0 \leqslant t < dP_{time} + P_{1dur} \\ K_{str} \cdot \frac{P_{vs0} - K_{vs} \cdot P_s(t) + P_3(t)}{P_{as}(t)} \\ \quad \text{if } dP_{time} + P_{1dur} \leqslant t \leqslant dP_{time} + dP_{dur} + P_{3dur} \\ K_{str} \cdot \frac{P_{vs0} - K_{vs} \cdot P_s(t) + P_3(t) + P_{4amp}}{P_{as}(t)} \\ \quad \text{if } dP_{time} + dP_{dur} + P_{3dur} < t \leqslant dP_{time} + dP_{dur} + P_{3dur} + P_{4dur} \\ K_{str} \cdot \frac{P_{vs0} + K_{vs} \cdot P_s(t) + P4amp/5}{P_{as}(t)} \\ \quad \text{if } t > dP_{time} + dP_{dur} + P_{3dur} + P_{4dur} \end{cases} \tag{17}$$

where P_{4dur} is the duration (s) of phase 4 and P_{4amp} is the amplitude of pressure (mmHg) increase that addresses the overshoot of the stroke volume in phase 4.

3.5.2 *Dermal system*

To simulate the phasic component of the EDA a second-order differential equation is used (according to [84]) to imitate both the diffusion of sweat via the sweat ducts and the evaporation from the skin. The EDA is stimulated by sympathetic activity, therefore the sympathetic tone T_{sym} is taken as an input:

$$\tau_r \tau_d \ddot{y}_p(t) + (\tau_r + \tau_d)\dot{y}_p(t) + y_p(t) = T_{sym}(t). \tag{18}$$

Here, τ_r is the rise time (s) for each SCR, τ_d the decay time (s), and y_p is the phasic component (µS) of the Skin Conductance signal. τ_r and τ_d were directly taken from [84].

3.6 PARAMETER ESTIMATION

The parameters introduced in the mathematical method were estimated by training them. To do so the `MATLAB` function `fminsearchbnd` was used which performs bound-constrained optimization using `fminsearch`[89]. Boundaries and initial parameters were taken from [9]. `fminsearch` makes use of the Nelder Mead[90] method. This method creates a simplex (with $n + 1$ vertices) using the provided initial n parameters and perturbing them slightly. The algorithm takes the following steps:

1. The points are sorted according to their function values from lowest to highest.
2. The centroid of all points except the worst point is calculated.
3. The 'worst' point is reflected through this centroid.
4. If the reflected point is better than the best, expand in this direction. Use the best one out of the expanded and reflected points.
5. In case the reflected point is worse than the worst point, contract towards the centroid. Assuming that the contracted point is better than the worst, go to step 1 again. On the other hand, if the contracted point is not better, execute a 'shrink'. Replace all points (except for the best point) with points closer to the best point.

6. Repeat these steps until the simplex remains almost constant. Ideally, the iterative cycle should be terminated when the function to be optimized, falls below a predefined tolerance. However, this is rarely the case. Instead, the algorithm is often terminated after a maximum number of iterations or when the change in function values is small enough.

An example of one iterative cycle for a two-dimensional problem can be seen in fig. 8.

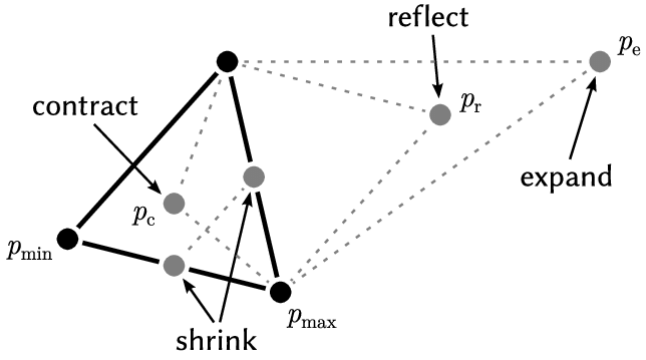

Figure 8: An iteration of the Nelder-Mead algorithm in two-dimensional space[91].

Subsequently, the model was trained on the average of Tertoolen's dataset and separately on the average of the dataset of 2024. Standard deviations were calculated to quantify the amount of variation in the distribution of the data around the mean. To personalize the model the H_0 and $\alpha SKNA_0$ can be changed (based on average HR and αSKNA before performing the VM). The final estimated parameters can be found in chapter 4.

MODEL ASSESSMENT

The following statistical measures were calculated to evaluate the model: the coefficient of determination, R^2, Root Mean Squared Error, RMSE, and the normalized RMSE. They can be seen in table 6. The coefficient of determination[92], R^2 was calculated using

$$\begin{aligned} R^2 &= 1 - \frac{SS_{res}}{SS_{tot}} \\ &= 1 - \frac{\sum_i \left(y_{pred}(i) - y_{meas}(i)\right)^2}{\sum_i \left(y_{meas}(i) - \bar{y}_{meas}\right)^2}. \end{aligned} \tag{19}$$

Here, SS_{res} is the residual sum of squares, SS_{tot} is the total sum of squares, y_{pred} indicates the predicted signal, and y_{meas} is the measured signal. The R-squared value measures the goodness of fit of a model and ranges from zero to one (where 1 indicates a perfect fit).
The RMSE[93] (as the name suggests) was determined as

$$RMSE = \sqrt{\frac{\left(\sum_{i=10}^{T} y_{pred}(i) - y_{meas}(i)\right)^2}{T}}. \tag{20}$$

The RMSE was taken over an appropriate epoch (from $t = 10$s onward) to minimize the effects of previous or posterior activities on measured data and sufficiently long after model initialization. An RMSE of zero indicates a perfect fit. The NRMSE[94] was normalized with respect to the range, in the following manner

$$NRMSE = \frac{RMSE}{max(y_{meas}) - min(y_{meas})}. \tag{21}$$

The NRMSE ranges from zero to one if the predicted data is in the same range as the measured data. Here, again zero indicates a perfectly fitted model.

In summary, the methodology provided details on the experiments of Tertoolen and this research, where ECG and EDA were recorded of subjects performing the VM and posture changes. A schematic overview outlined the signal processing workflow used to retrieve HR, SKNA, aSKNA, and the phasic and tonic components of EDA. The proposed model integrated the cardiovascular system, baroreceptors, ANS, and skin. A mathematical model was presented with differential equations for the arterial systemic pressure, the firing rate of the baroreceptors and the phasic component of the EDA. Lastly, the chapter described the parameter estimation method.

4

RESULTS

In the following section, the results of the experiments that were conducted are shown. Moreover, a comparison is made between the modelled HR, aSKNA, and EDA, and those measured features from Tertoolen's dataset. Furthermore, the acquired dataset (heart rate and aSKNA data) is compared to the predicted signals.

RESULTS STUDY 2023, TERTOOLEN

In fig. 9 the mean with standard deviations over the features of interest can be seen for Study 2023, the pilot dataset of Tertoolen. The aSKNA response to the VM precedes the heart rate and EDA response.

Subsequently, these average data were used to train the model parameters. This can be seen in fig. 10. An example of these features for individual subjects over the entire timeline can be seen in the appendix A in figs. 16 to 21. The heart rate and aSKNA predictions seem to follow the measured data quite nicely. The (mean) EDA amplitude exhibits fluctuations, contrasting with the smoother EDA prediction, but overall the trend is similar.

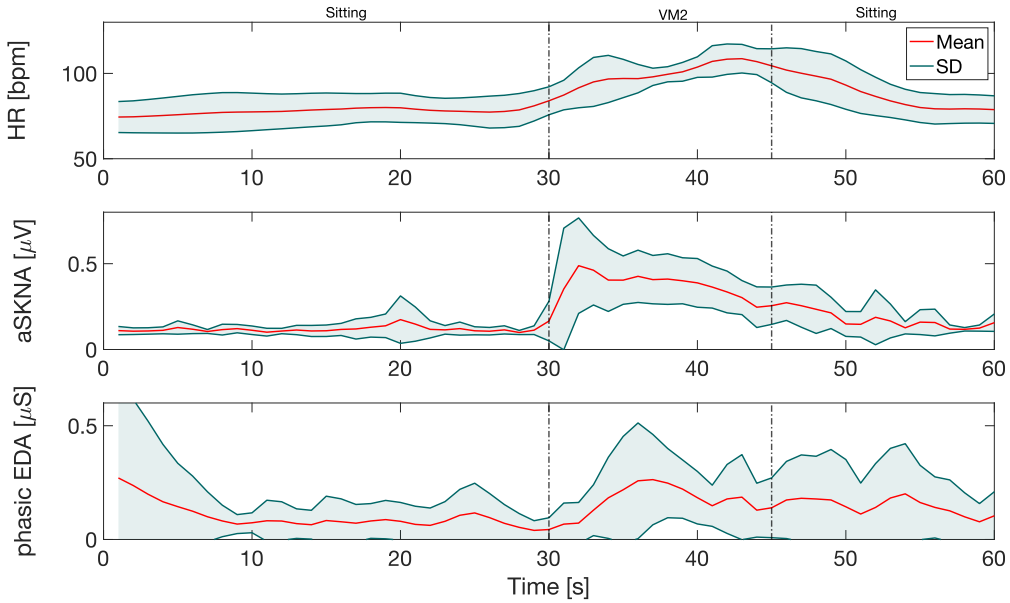

Figure 9: Mean (red) measured heart rate, aSKNA, and the phasic component of EDA for Tertoolen's pilot dataset shown over time, where the VM is performed at t = 30 s for 15 s. During this epoch, the subject was sitting and performed the second VM. The green areas indicate the standard deviation.

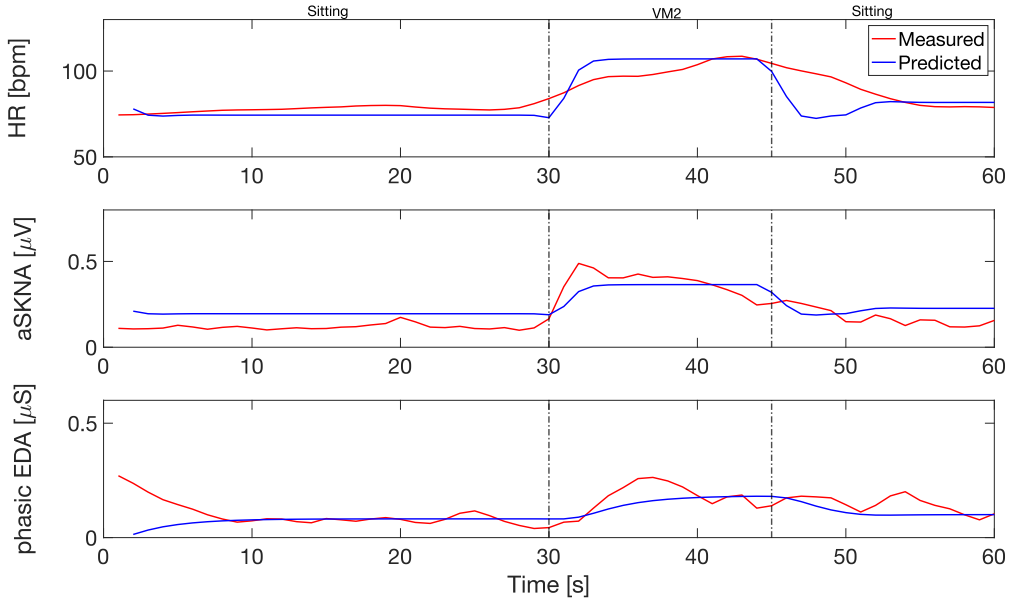

Figure 10: Predicted (blue) and measured (red) mean heart rate, aSKNA, and the phasic component of EDA over time. The measured data is from Study 2023, Tertoolen's pilot dataset. The subject was sitting and performed the Valsalva Manoeuvre between 30 and 45 s.

RESULTS STUDY 2024

Below, the results of Study 2024 are presented. Due to a technical issue with the Refa, the sampling frequency of the ECG data was in question. This will be discussed in more detail in chapter 5. Thus, data processing was carried out using both assumed sampling frequencies: 2048 and 1250 Hz. The results of this analysis are given here. The final estimated parameters and the general parameters can be found in tables 7 and 8.

Sampling frequency 2048 Hz

First, the results are given with an assumed sampling frequency of 2048 Hz. Figure 11 shows the mean measured heart rate and aSKNA data with standard deviation for the acquired dataset, Study 2024. The plot depicts the VM during standing. Prior, the activities of lying down, sitting, and the initial VM were performed. Unfortunately, EDA data was not recorded for all subjects and the acquired EDA data was not up to standards. Moreover, the alignment between the Refa and E4 data was somewhat unclear. Consequently, it was difficult to determine the exact timing of the experiment activities. The individual results per subject can be seen in appendix A.2.2.

The baseline heart rate for Study 2024 is higher than for Study 2023 with an average of 138 bpm and 82 bpm, respectively. The aSKNA data is more comparable, although the peak amplitude of 2024 exceeds that of 2023, 0.56 µV versus 0.43 µV. The standard deviation for 2024 is a bit larger than in 2023 due to the wider spread of data.

In fig. 12 the model versus measured data from Study 2024 can be seen. The model was again optimized, but this time using the mean dataset of 2024. The model predicts a lower baseline heart rate. The aSKNA prediction shows a delayed response. When comparing the

aSKNA data from both Study 2024 and Study 2023, it reveals that the VM initially triggers a sharp response that gradually decreases. This behaviour is less pronounced in the predicted aSKNA data. Moreover, the model predicts a simultaneous (or even a delayed) response of the aSKNA and heart rate to the VM, while all measured data suggested only a delayed heart rate response.

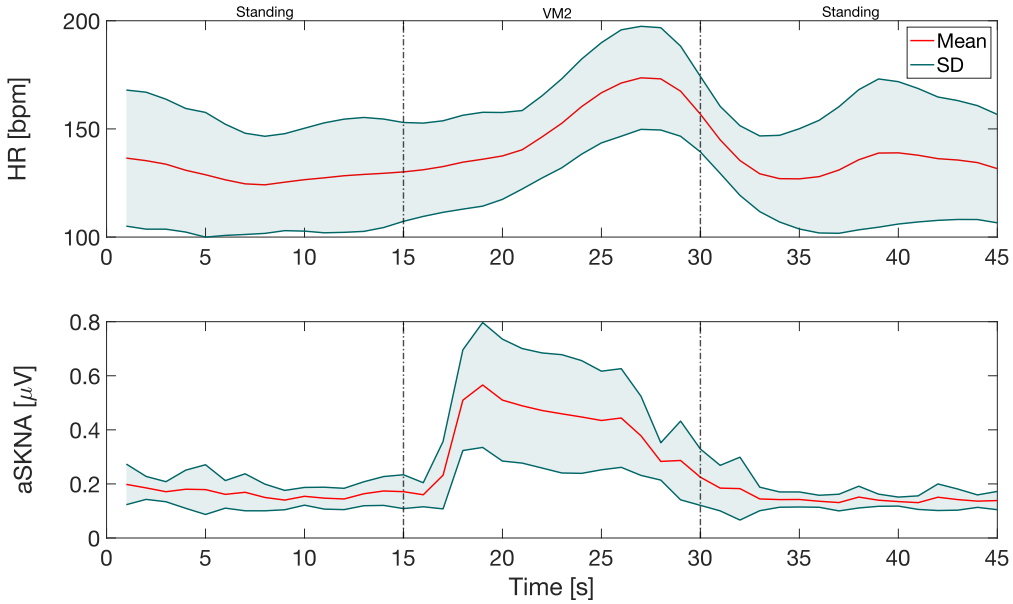

Figure 11: Mean (red) measured heart rate and aSKNA for the dataset of 2024 shown over time, where the VM is performed at t = 15 s for 15 s. During this epoch, the subject was standing. The green areas indicate the standard deviation.

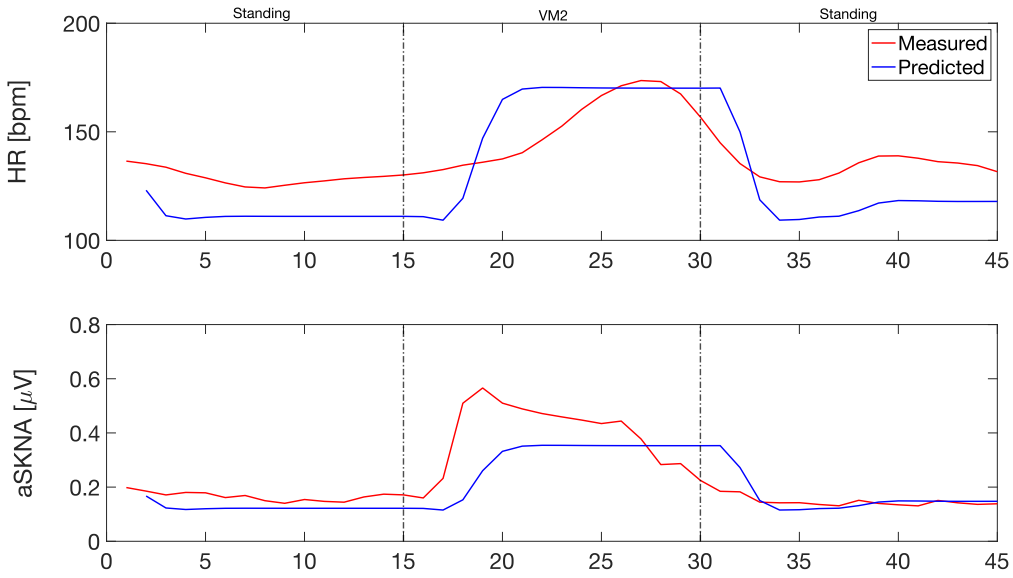

Figure 12: Predicted (blue) and measured (red) mean heart rate and aSKNA over time. The measured data is from the dataset acquired in 2024. The subject was standing and performed the Valsalva Manoeuvre between 15 and 30 s.

Sampling frequency 1250 Hz

Here, the results are provided with an assumed sampling frequency of 1250 Hz. Consequently, it was not possible to use a bandpass filter with a bandwidth of 500 to 1000 Hz. Therefore, SKNA data was acquired by filtering between 500 and 625 Hz.

Figure 13 shows the mean measured heart rate and aSKNA data with standard deviation for the acquired dataset, Study 2024. The plot depicts the VM during standing. Prior, the activities of lying down, sitting, and the initial VM were performed. The individual results per subject can be seen in appendix A.2.1.

Here, the baseline heart rate for Study 2024 is comparable to Study 2023, 73 and 82 bpm, respectively. This mean heart rate falls within a more physiologically expected range compared to the findings from Study 2024 (2048 Hz). The aSKNA peak amplitude is considerably lower, 0.19 µV, compared to 0.43 µV in Study 2023.

In fig. 14 the model versus the (in 2024) measured data can be seen. The model was again optimized using the mean dataset of 2024. The model predicts an expedited heart rate response compared to the measured heart rate data, while the aSKNA prediction shows a delayed response relative to measured aSKNA data. The predicted heart rate response occurs faster than the predicted aSKNA response to the VM. This is in contrast with measured data.

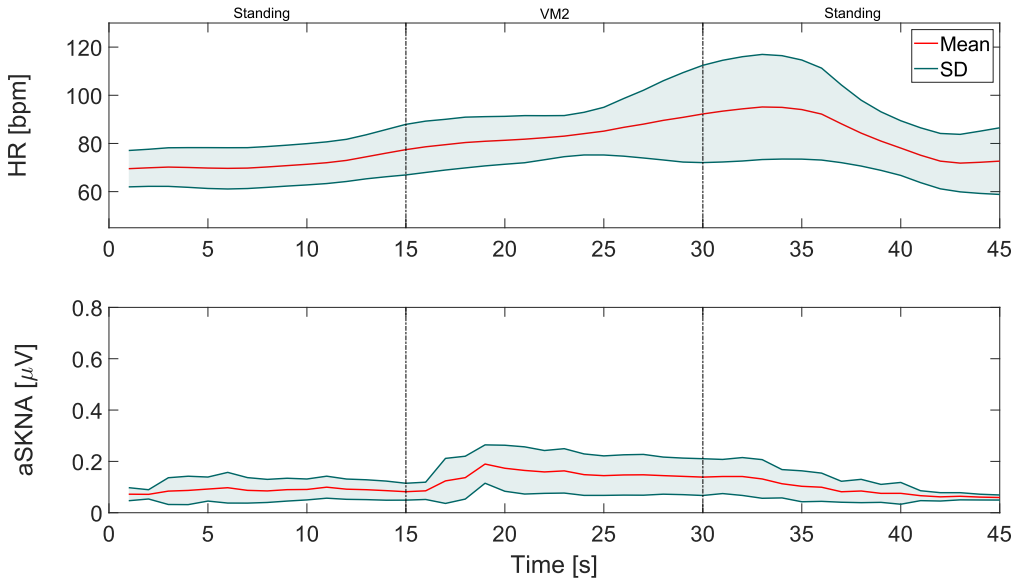

Figure 13: Mean (red) measured heart rate and aSKNA for Study 2024 shown over time, where the VM is performed at t = 15 s for 15 s. During this epoch, the subject was standing. The green areas indicate the standard deviation.

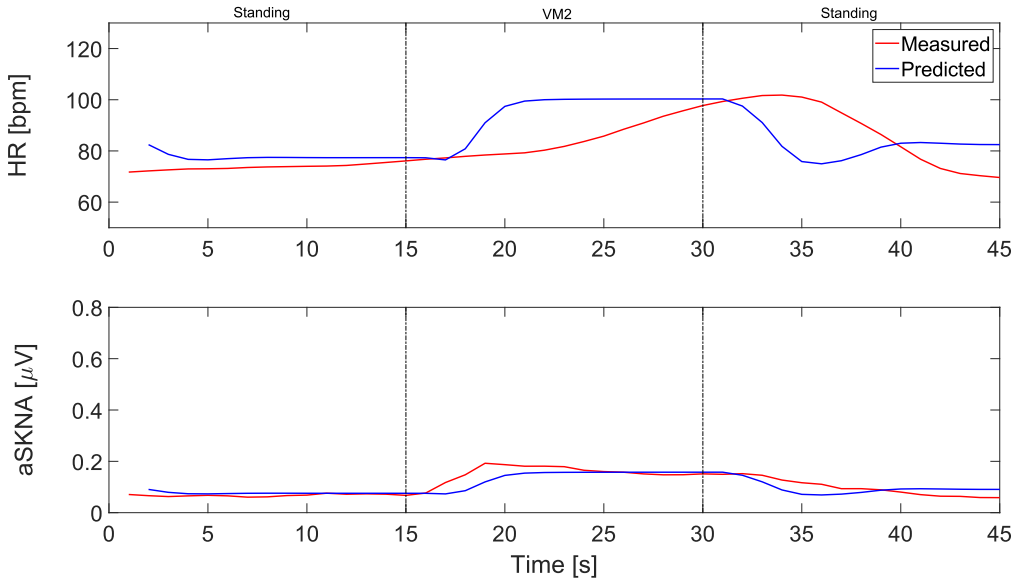

Figure 14: Predicted (blue) and measured (red) mean heart rate and aSKNA over time. The measured data is from Study 2024. The subject was standing and performed the Valsalva Manoeuvre between 15 and 30 s.

MODEL PERFORMANCE

Table 6 shows the model performance using the coefficient of determination, R^2, the Root Mean Squared Error, RMSE, and the normalized RMSE.

Table 6: Comparison of model performance using the coefficient of determination (R^2), the Root Mean Squared Error (RMSE), and Normalized Root Mean Squared Error (NRMSE) on Tertoolen's dataset and the acquired dataset.

	R^2	RMSE	NRMSE
Mean 2023 Tertoolen			
HR	0.623	8.790 bpm	0.257
aSKNA	0.770	0.075 µV	0.193
EDA	0.587	0.041 µS	0.041
Mean 2024 (2048 Hz)			
HR	0.694	17.605 bpm	0.356
aSKNA	0.486	0.115 µV	0.264
Mean 2024 (1250 Hz)			
HR	0.075	12.368 bpm	0.379
aSKNA	0.692	0.027 µV	0.199

The coefficient of determination mainly assesses the shape of the plot and its fit to the model, placing less emphasis on the difference in average amplitude. The model performs best on Study 2023 (Tertoolen's dataset) according to the R-squared values. This is also true according to the NRMSE. The aSKNA prediction is most comparable over both studies (and for both assumed sampling rates for Study 2024), with R-squared values between 0.486 and 0.770.

However, especially heart rate prediction for Study 2024 (with an assumed sampling frequency of 1250 Hz) falls short, with an extremely low value for the coefficient of determination, 0.075, and a somewhat high NRMSE, 0.379. This results mainly from the difference in timing. The lowest NRMSE value, 0.041, is reported in the EDA assessment. However, the corresponding coefficient of determination is only 0.587.

Table 7: General model parameters.

General	Definition	Value	Unit
N_0	Minimum threshold baroreceptors firing rate	35 [9]	Hz
M	Maximum baroreceptors firing rate	120 [9]	Hz
$P_{s_{max}}$	Maximum intra-thoracic pressure	40 [9]	mmHg
dP_{dur}	Duration of forced expiration (VM)	15	s
τ_r	Rise time SCR	0.73 [84]	s
τ_d	Decay time SCR	2.86 [84]	s

In summary, this results chapter showed good correspondence based on statistical and visual comparison between the modelled and measured features: heart rate, aSKNA, and EDA. However, the clear faster response of the sympathetic activity compared to SCR and heart rate response in measured data was not reflected by the model. However, the predictions did show similarity with measurements, especially for the model trained on Tertoolen's dataset.

Table 8: Final estimated parameters for each dataset.

Parameter	Definition	Study 2023	Study 2024 (fs = 2048 Hz)	Study 2024 (fs = 1250 Hz)	Unit
β	Dampening factor	1.36	1.39	1.40	
C_{as}	Arterial systemic compliance	0.10	0.10	0.15	L/mmHg
τ	Time constant	3.21	3.45	3.47	s
K	Weighting factor	0.94	0.95	0.96	Hz/mmHg
H_0	Mean heart rate	89.81	100.00	84.75	bpm
$P_{as_{mean}}$	Mean arterial systemic pressure	116.47	117.62	119.96	mmHg
$aSKNA_0$	Baseline aSKNA	0.06	0.05	0.02	µV
K_{aSKNA}	Scaling factor aSKNA	5.90	6.40	6.29	
M_p	Scaling factor parasympathetic response	0.71	0.08	0.38	
M_s	Scaling factor sympathetic response	0.11	0.82	0.22	
P_{vs_0}	Mean venous systemic pressure before VM	9.42	9.97	10.02	mmHg
K_{vs}	Weighting factor for the venous systemic pressure	0.34	0.32	0.33	
PR_0	Baseline peripheral resistance	6.24	6.55	6.58	mHgmin/L
K_{PR}	Scaling factor peripheral resistance	3.19	1.80	3.2	
K_{str}	Weighting factor stroke volume	0.92	0.94	0.94	L/b
P_{1dur}	Duration phase 1	2.09	2.13	2.13	s
R_{1amp}	Amplitude resistance increase in phase 1	2.57	2.73	2.74	mmHgmin/L
P_{3dur}	Duration phase 3	3.59	3.72	3.73	second
P_{3amp}	Amplitude of pressure drop in phase 3	2.60	2.69	2.70	mmHg
P_{4dur}	Duration phase 4	2.35	2.42	2.43	s
P_{4amp}	Amplitude of pressure increase in phase 4	4.12	4.21	4.21	mmHg
dP_{time}	Timestamp start VM	28	15	15	s
dP_{rate}	Growing rate pressure	5.00	5.00	5.00	

5

DISCUSSION & RECOMMENDATIONS

In this exploratory research, a model was proposed to predict the ANS response to the performance of a VM. The features modelled were heart rate, aSKNA, and the phasic tone of EDA. The model was trained on the mean data of Tertoolen's dataset and the dataset acquired during this research. In chapter 4 the results were given of the measured as well as predicted data.

INCONSISTENCY SAMPLING FREQUENCY STUDY 2024

As briefly mentioned in chapter 4, the sampling frequency of the ECG data was called into question. The analyzed data yielded unusually high heart rates that fell outside the expected physiological range for this type of experiment. By calculating the frequency using the known start and end timestamps and the number of samples, the sampling frequency was determined to be approximately 1250 Hz. Upon reviewing the system specifications (see fig. 45), it became evident that a sampling frequency of 2048 Hz was not an available option. Instead, the system allowed for frequencies of among others, 1250 Hz and 2500 Hz. After a collaborative discussion with TMSi[95], we reached the conclusion that the Refa device likely operated at the nearest possible sampling frequency (rounded down), which was a sampling frequency of 1250 Hz.
It is highly likely that the 1250 Hz data is correct. Therefore, it seems most logical to focus on discussing and interpreting these results further.

DISCUSSION OF RESULTS

The measured data from Study 2023 and Study 2024 (with a sampling frequency of 1250Hz) indicated that the heart rate and phasic EDA display a delayed response to the autonomic function test, while the sympathetic response precedes. This can be explained by the fact that sympathetic activity triggers the increase in heart rate and stimulates the eccrine sweat glands, resulting in a rise in phasic EDA. Both of these processes might require a short period of time.

For both experiments, the second VM was chosen to depict. For Study 2023, Tertoolen's experiment, this was after performing the following activities; lying, VM, lying, and sitting. Yet, for our experiment, Study 2024, the subjects performed the following activities; lying, VM, sitting, and standing. From figs. 23, 24 and 27 in appendix A.2.1, it can be observed that the heart rate did not always return to baseline after each activity. Likely, the time provided for heart rate recovery between activities was inadequate.

The aSKNA signal returns to baseline after each activity because the SNS responds rapidly and its activity is short-lived. However, the amplitude of the measured aSKNA responses varied between studies. This difference may be due to variations in filtering parameters. In Study 2024, data could only be filtered between 500 and 625 Hz, because the sampling frequency was 1250 Hz. This limited the maximum frequency that could be accurately analyzed (known as

the Nyquist frequency). In contrast, in Study 2023, SKNA was analyzed with a bandpass filter between 500 and 1000 Hz, allowing a broader frequency range. Besides, Tertoolen also stated in her thesis that a sampling frequency above 2000 Hz was required to overcome aliasing.

Regarding the EDA results, it can be said that the effect of the VM is not as clear as in the literature, as illustrated in [49], and has a large variation in amplitude, thus it also has a quite large standard deviation interval. Perhaps the processing of EDA data can be refined. Moreover, the quality of EDA might be lower, although both Tertoolen and Baghestani et al. collected EDA signals from the index and middle finger. Unfortunately, the EDA data from Study 2024 was of lower quality. This might be explained by the signal being recorded on the wrist (using the Empatica E4). Eccrine sweat glands are primarily located on the palms of the hands, soles of the feet, forehead and armpits[65]. Therefore, wrist-worn devices to record EDA seem less reliable (though Mee et al.[96] saw that wrist-based measurements of EDA demonstrated directional consistency with palm-based measurements but had modest correlations with them). Lastly, the EDA data was not recorded consistently for all subjects and the timing alignment between the E4 (EDA) data and Refa (ECG) data was unclear. Baghestani et al. observed an average delay in EDA burst onset of 4.6 s compared to the iSKNA burst. This makes the alignment between data even more difficult. A solution for this could be to trigger all signals by starting with a VM. Following this, a sufficiently long recovery period should be provided, after which the actual protocol could be executed.

The simulated features (figs. 10 and 14) are quite promising and show similarity to measured data. Especially the simulated sympathetic activity, as reflected by the simulation of aSKNA, compared to Study 2023, Tertoolen's dataset, shows potential judging by the reported (table 6) high R-squared value (0.770) and the NRMSE (0.193). However, the baseline aSKNA should be adjusted lower based on measured data (from Study 2023). The reported statistical measures for Study 2024 show a reduced performance for heart rate prediction, but a comparable performance for aSKNA prediction. The timing of the heart rate response is particularly complex.

It is evident that the shape of measured and predicted data differ somewhat. The reason for this could be incorrect model parameters and the level of simplification of the model. Specifically, as stated in chapter 2, the SNS is involved in a more complex process and thus exhibits a delayed response compared to the PSNS, with a typical delay of 4 to 7 s[32]. This delay, as incorporated by Ottesen and Olufsen[32], was not included in our model, which significantly impacts the timing of the heart rate, aSKNA, and EDA responses. I have shortly experimented with incorporating a time delay in the Simulink model. However, this introduced instability into the system. Specifically, the heart rate showed fluctuations as it tried to reach equilibrium, and the system demonstrated considerable oscillations when the VM was applied as a disturbance. This suggests that while timing is important, it must be carefully integrated to avoid negatively affecting model performance.
The model aims to simulate a general response to the VM. The model parameters are expected to improve with additional time. Perhaps employing a different optimization technique or function, rather than `fminsearch`, could reduce computation time. Additionally, exploring alternative approaches, such as machine learning, may lead to a more accurate model, though it poses the risk of overfitting.

RECOMMENDATIONS

Looking back on the experiments, it is recommended to change the study design. Sufficient recovery time should be incorporated between stimuli (e.g. waiting 30 s or more after VM to stand up). This adjustment would prevent the VM from influencing the response to standing up, and vice versa, thereby also improving the accuracy of data analysis. Besides, this makes it easier to model. Furthermore, as the model predicts a response to the VM, only the VM should be tested. The postural changes are not the focus of this study, but various static postures could be incorporated in different sessions. Lastly, I would invest more time into the integration of the time delay for the sympathetic tone compared to the parasympathetic tone into the model.
Finally, I would suggest incorporating blood pressure measurements into the protocol. This additional input (along with the timing of the VM, which is now the only input), could enhance the model and improve its physiological accuracy. I was unable to do so due to equipment being unavailable.

6

CONCLUSION

In this thesis, the autonomic cardiac regulation was explored by evaluating the sympathetic response to the Valsalva Manoeuvre in ten participants. A simplified model was developed to simulate three features related to sympathetic activity: aSKNA, heart rate, and phasic tone of EDA. The model parameters were trained on the mean data from a previously obtained dataset from Tertoolen[1], Study 2023, and on the mean data from the dataset acquired during this research, Study 2024.

Finally, the predicted features showed useful similarity to the measured signals; however, statistical analysis indicated room for improvement. The heart rate prediction on the dataset of Study 2023 was quite promising with an adequate R-squared value of 0.623 and an RMSE normalized with respect to the range of 0.257. Heart rate prediction on the dataset of Study 2024 (sampled at 1250 Hz) lacked timing precision, leading to an R-squared value of 0.075, and an NRMSE of 0.379. However, aSKNA prediction on both datasets was satisfactory with reported R-squared values of 0.770 (Study 2023) and 0.692 (Study 2024), and NRMSEs of 0.193 (Study 2023), and 0.199 (Study 2024). EDA prediction results (for Study 2023) were also encouraging with an R-squared value of 0.587 and NRMSE of 0.041.
The model predicted simultaneous heart rate and aSKNA responses to the VM, whereas measured data showed a delayed heart rate response. The model did not incorporate the difference in timing between the sympathetic response and the faster parasympathetic response.

Consequently, further model and parameter optimization is necessary, potentially incorporating machine learning and the delay in sympathetic response. Additionally, integrating measured blood pressure signals could enhance the model's accuracy. In conclusion, this study presents a well-simplified initial attempt at modelling autonomic cardiac control, resulting in heart rate, aSKNA, and EDA simulations comparable with experimental data. This resemblance gave insight into the functioning of autonomic cardiac regulation and laid a foundation for future research.

BIBLIOGRAPHY

[1] Jacomine Tertoolen. 'Evaluation of the Cardiac Tone by Sympathetic Skin Nerve Activity.' In: *Masterthesis* (2023).

[2] Brain & Spine specialists. *Nervous System Facts: Human Nerves Explained*. 2023. URL: https://brainandspinecenterllc.com/2023/06/23/how-many-nerves-are-in-the-human-body/#:~:text=Divingintotheworldof,toabody'selectricalwiring..

[3] Office of Communications. *What are the parts of the nervous system?* 2018. URL: https://www.nichd.nih.gov/health/topics/neuro/conditioninfo/parts#:~:text=Thecentralnervoussystemis,allpartsofthebody..

[4] Thomas H. Everett, Anisiia Doytchinova, Yong-Mei Cha, and Peng-Sheng Chen. 'Recording Sympathetic Nerve Activity from the Skin.' In: *Trends Cardiovasc Med.* 1 (2018), 463–472. DOI: 10.1016/j.tcm.2017.05.003..

[5] Ting Yu Li, Wei Chung Tsai, and Shien Fong Lin. 'Non-invasive Recording of Parasympathetic Nervous System Activity on Auricular Vagal Nerve Branch.' In: *Proceedings of the Annual International Conference of the IEEE Engineering in Medicine and Biology Society, EMBS* 2020-July (2020), pp. 4337–4340. ISSN: 1557170X. DOI: 10.1109/EMBC44109.2020.9176098.

[6] Xiao Liu et al. 'Skin sympathetic nerve activity as a biomarker of fitness.' In: *Heart Rhythm* 18.12 (2021), pp. 2169–2176. ISSN: 15563871. DOI: 10.1016/j.hrthm.2021.08.031.

[7] Anisiia Doytchinova et al. 'Simultaneous noninvasive recording of skin sympathetic nerve activity and electrocardiogram.' In: *Heart Rhythm* 14.1 (2017), pp. 25–33. ISSN: 15563871. DOI: 10.1016/j.hrthm.2016.09.019. URL: http://dx.doi.org/10.1016/j.hrthm.2016.09.019.

[8] Ilya A. Rybak, Yaroslav I. Molkov, Julian F.R. Paton, Ana P.L. Abdala, and Daniel B. Zoccal. 'Modeling the Autonomic Nervous System.' In: *Primer on the Autonomic Nervous System* (2012), pp. 681–687. DOI: 10.1016/B978-0-12-386525-0.00143-8.

[9] Michel Kana and Jiri Holcik. 'Mathematical model-based markers of autonomic nervous activity during the Valsalva Maneuver and comparison to heart rate variability.' In: *Biomedical Signal Processing and Control* 6.3 (2011), pp. 251–260. ISSN: 17468108. DOI: 10.1016/j.bspc.2011.05.001. URL: http://dx.doi.org/10.1016/j.bspc.2011.05.001.

[10] Takashi Kusayama et al. 'Simultaneous noninvasive recording of electrocardiogram and skin sympathetic nerve activity (neuECG).' In: *Nature Protocols* 15.5 (2020), pp. 1853–1877. ISSN: 17502799. DOI: 10.1038/s41596-020-0316-6. URL: http://dx.doi.org/10.1038/s41596-020-0316-6.

[11] K Yamamoto, G Sobue, S Iwase, T Mitsuma, and T Mano. '[Skin sympathetic nerve activity in amyotrophic lateral sclerosis].' In: *Rinsho shinkeigaku = Clinical neurology* 34.4 (Apr. 1994), pp. 377–80. ISSN: 0009-918X.

[12] Stian Roti Svendby. *MATHEMATICAL MODELLING OF HEART RATE DURING CYCLING EXERCISE*. Tech. rep. 2016.

[13] Maarten Thoonen, Peter Veltink, Frank Halfwerk, Robby Van Delden, and Ying Wang. 'A Movement-Artefact-Free Heart-Rate Prediction System.' In: *Computing in Cardiology* 2022-Septe (2022), pp. 1–4. ISSN: 2325887X. DOI: 10.22489/CinC.2022.190.

[14] Yurii M. Ishbulatov, Anatoly S. Karavaev, Anton R. Kiselev, Margarita A. Simonyan, Mikhail D. Prokhorov, Vladimir I. Ponomarenko, Sergey A. Mironov, Vladimir I. Grid-

nev, Boris P. Bezruchko, and Vladimir A. Shvartz. 'Mathematical modeling of the cardiovascular autonomic control in healthy subjects during a passive head-up tilt test.' In: *Scientific Reports* 10.1 (Dec. 2020). ISSN: 20452322. DOI: 10.1038/s41598-020-71532-7.

[15] Francis J. Doyle, Michael A. Henson, Babatunde A. Ogunnaike, James S. Schwaber, and Ilya Rybak. *Neuronal Modeling of the Baroreceptor Reflex with Applications in Process Modeling and Control*. Woodhead Publishing Limited, 1997, pp. 87–127. DOI: 10.1016/b978-012526430-3/50006-4. URL: http://dx.doi.org/10.1016/B978-012526430-3/50006-4.

[16] Mette S Olufsen, Hien T Tran, Johnny T Ottesen, Research Experiences, Undergraduates Program, Lewis A Lipsitz, and Vera Novak. 'Modeling baroreflex regulation of heart rate during orthostatic stress.' In: *Am J Physiol Regul Integr Comp Physiol* 291 (2006), pp. 1355–1368. DOI: 10.1152/ajpregu.00205.2006.-During. URL: http://www.ajpregu.org.

[17] Mette S. Olufsen, April V. Alston, Hien T. Tran, Johnny T. Ottesen, and Vera Novak. 'Modeling heart rate regulation - Part I: Sit-to-stand versus head-up tilt.' In: *Cardiovascular Engineering* 8.2 (2008), pp. 73–87. ISSN: 15678822. DOI: 10.1007/s10558-007-9050-8.

[18] Jacob Sturdy, Johnny T. Ottesen, and Mette S. Olufsen. 'Modeling the differentiation of A- and C-type baroreceptor firing patterns.' In: *Journal of Computational Neuroscience* 42.1 (Feb. 2017), pp. 11–30. ISSN: 15736873. DOI: 10.1007/s10827-016-0624-6.

[19] Maxwell Lewis Neal and James B. Bassingthwaighte. 'Subject-specific model estimation of cardiac output and blood volume during hemorrhage.' In: *Cardiovascular Engineering* 7.3 (Sept. 2007), pp. 97–120. ISSN: 15678822. DOI: 10.1007/s10558-007-9035-7.

[20] Fuyou Liang and Hao Liu. 'Simulation of hemodynamic responses to the Valsalva maneuver: An integrative computational model of the cardiovascular system and the autonomic nervous system.' In: *Journal of Physiological Sciences* 56.1 (Feb. 2006), pp. 45–65. ISSN: 18806546. DOI: 10.2170/physiolsci.RP001305.

[21] K. Hemalatha and M. Manivannan. 'Valsalva maneuver for the analysis of interaction hemodynamic - Model study.' In: *ITC 2010 - 2010 International Conference on Recent Trends in Information, Telecommunication, and Computing*. 2010, pp. 28–32. ISBN: 9780769539751. DOI: 10.1109/ITC.2010.54.

[22] Jennie Tsao, Subhadra Evans, Laura Seidman, Lung, Lonnie Zeltzer, and Bruce Naliboff. 'Heart rate variability as a biomarker for autonomic nervous system response differences between children with chronic pain and healthy control children.' In: *Journal of Pain Research* (June 2013), p. 449. ISSN: 1178-7090. DOI: 10.2147/JPR.S43849.

[23] Chandra Mohan Kumar and André A J Van Zundert. 'Intraoperative Valsalva maneuver: a narrative review.' eng. In: *Canadian journal of anaesthesia = Journal canadien d'anesthesie* 65.5 (May 2018), pp. 578–585. ISSN: 1496-8975 (Electronic). DOI: 10.1007/s12630-018-1074-6.

[24] Simulink Documentation. *Simulation and Model-Based Design*. 2024. URL: https://www.mathworks.com/products/simulink.html.

[25] Dr. Qaiswer Shah Lakanwal and Dr. Mujahed Hematyar. 'Autonomic nervous system anatomy.' In: *International Journal of Advanced Academic Studies* 3.3 (2021), pp. 130–135. ISSN: 27068919. DOI: 10.33545/27068919.2021.v3.i3b.590.

[26] ScienceDirect. *Lie Detection - an overview*. 2013. URL: https://www.sciencedirect.com/topics/nursing-and-health-professions/lie-detection#:~:text=Lie%20detection%20is%20based%20on,questioned%20by%20a%20trained%20examiner.

[27] John Synnott, David Dietzel, and Maria Ioannou. 'A review of the polygraph: history, methodology and current status.' In: *Crime Psychology Review* 1.1 (Jan. 2015), pp. 59–83. ISSN: 23744014. DOI: 10.1080/23744006.2015.1060080.

[28] National Research Council. *The Polygraph and Lie Detection*. Washington, DC: The National Academies Press, 2003.

[29] S. Braune, A. Hetzel, A. Prasse, K. Dohms, B. Guschlbauer, and C. H. Lücking. 'Stimulation of sympathetic activity by carbon dioxide in patients with autonomic failure compared to normal subjects.' In: *Clinical Autonomic Research* 7.6 (Dec. 1997), pp. 327–332. ISSN: 0959-9851. DOI: 10.1007/BF02267726.

[30] Jens Jordan, John R. Shannon, Andre Diedrich, Bonnie Black, Fernando Costa, David Robertson, and Italo Biaggioni. 'Interaction of Carbon Dioxide and Sympathetic Nervous System Activity in the Regulation of Cerebral Perfusion in Humans.' In: *Hypertension* 36.3 (Sept. 2000), pp. 383–388. ISSN: 0194-911X. DOI: 10.1161/01.HYP.36.3.383.

[31] Francesco Onorati, Riccardo Barbieri, Maurizio Mauri, Vincenzo Russo, and Luca Mainardi. 'Reconstruction and analysis of the pupil dilation signal: Application to a psychophysiological affective protocol.' In: *2013 35th Annual International Conference of the IEEE Engineering in Medicine and Biology Society (EMBC)*. IEEE, July 2013, pp. 5–8. ISBN: 978-1-4577-0216-7. DOI: 10.1109/EMBC.2013.6609423.

[32] J. T. Ottesen and M. S. Olufsen. 'Functionality of the baroreceptor nerves in heart rate regulation.' In: *Computer Methods and Programs in Biomedicine* 101.2 (2011), pp. 208–219. ISSN: 01692607. DOI: 10.1016/j.cmpb.2010.10.012. URL: http://dx.doi.org/10.1016/j.cmpb.2010.10.012.

[33] Stuart Ira Fox. *Human Physiology*. 10th ed. New York, NY: McGraw-Hill Education, 2008. ISBN: 9780073344331.

[34] Agnieszka Zygmunt and Jerzy Stanczyk. *Methods of evaluation of autonomic nervous system function*. 2010. DOI: 10.5114/aoms.2010.13500.

[35] C. J. Mathias, I. Corazza, P. Guaraldi, G. Barletta, and P. Cortelli. 'Autonomic nervous system: Clinical testing.' In: *The Curated Reference Collection in Neuroscience and Biobehavioral Psychology*. Elsevier Science Ltd., Jan. 2017, pp. 911–928. ISBN: 9780128093245. DOI: 10.1016/B978-0-12-809324-5.01817-4.

[36] David Chambers, Christopher Huang, and Gareth Matthews. *Basic Physiology for Anaesthetists. Section 3 Cardiovascular Physiology. Chapter 41 Valsalva Manoeuvre*. Cambridge University Press, July 2019, p. 175. ISBN: 9781108565011. DOI: 10.1017/9781108565011. URL: https://www.cambridge.org/core/product/identifier/9781108565011/type/book.

[37] I. Kutkut et al. 'Skin sympathetic nerve activity as a biomarker for neurologic recovery during therapeutic hypothermia for cardiac arrest.' In: *Heart rhythm* 18 (2021). DOI: 10.1016/j.hrthm.2021.03.011.

[38] Wenbo He, Yuzhu Tang, Guannan Meng, Danning Wang, Johnson Wong, Gloria A. Mitscher, David Adams, Thomas H. Everett, Peng-Sheng Chen, and Shalini Manchanda. 'Skin sympathetic nerve activity in patients with obstructive sleep apnea.' In: *Heart Rhythm* 17.11 (Nov. 2020), pp. 1936–1943. ISSN: 15475271. DOI: 10.1016/j.hrthm.2020.06.018. URL: https://linkinghub.elsevier.com/retrieve/pii/S1547527120305968.

[39] Nancy Gullett, Zuzanna Zajkowska, Annabel Walsh, Ross Harper, and Valeria Mondelli. 'Heart rate variability (HRV) as a way to understand associations between the autonomic nervous system (ANS) and affective states: A critical review of the literature.' In: *International Journal of Psychophysiology* 192 (Oct. 2023), pp. 35–42. ISSN: 01678760. DOI: 10.1016/j.ijpsycho.2023.08.001.

[40] Zhipeng Cai, Hongyi Cheng, Yantao Xing, Feifei Chen, Yike Zhang, and Chang Cui. 'Autonomic nervous activity analysis based on visibility graph complex networks and skin sympathetic nerve activity.' In: *Frontiers in Physiology* 13 (Sept. 2022). ISSN: 1664-042X. DOI: 10.3389/fphys.2022.1001415.

[41] Jiakun Li and Lihui Zheng. *The Mechanism of Cardiac Sympathetic Activity Assessment Methods: Current Knowledge*. June 2022. DOI: 10.3389/fcvm.2022.931219.

[42] Yantao Xing et al. 'Design and evaluation of an autonomic nerve monitoring system based on skin sympathetic nerve activity.' In: *Biomedical Signal Processing and Control* 76 (July 2022), p. 103681. ISSN: 17468094. DOI: 10.1016/j.bspc.2022.103681.

[43] Songwen Chen, Guannan Meng, Anisiia Doytchinova, Johnson Wong, Susan Straka, Julie Lacy, Xiaochun Li, Peng Sheng Chen, and Thomas H. Everett IV. 'Skin Sympathetic Nerve Activity and the Short-Term QT Interval Variability in Patients With Electrical Storm.' In: *Frontiers in Physiology* 12.December (2021). ISSN: 1664042X. DOI: 10.3389/fphys.2021.742844.

[44] T. C. Huang et al. 'Skin sympathetic nerve activity and ventricular arrhythmias in acute coronary syndrome.' In: *Heart Rhythm* 19 (2022). DOI: 10.1016/j.hrthm.2022.04.031.

[45] Andrew Lee, Xiao Liu, Carine Rosenberg, Sanjana Borle, Daerin Hwang, Lan S. Chen, Xiaochun Li, Noel Bairey Merz, and Peng-Sheng Chen. 'Skin sympathetic nerve activity in patients with chronic orthostatic intolerance.' In: *Heart Rhythm* 19.7 (July 2022), pp. 1141–1148. ISSN: 15475271. DOI: 10.1016/j.hrthm.2022.03.015. URL: https://linkinghub.elsevier.com/retrieve/pii/S1547527122002399.

[46] Daerin Hwang et al. 'Sympathetic toggled sinus rate acceleration as a mechanism of sustained sinus tachycardia in chronic orthostatic intolerance syndrome.' In: *Heart Rhythm* 19.12 (Dec. 2022), pp. 2086–2094. ISSN: 15475271. DOI: 10.1016/j.hrthm.2022.08.015. URL: https://linkinghub.elsevier.com/retrieve/pii/S1547527122023116.

[47] Yu Chen Chen et al. 'Skin sympathetic nerve activity as a potential biomarker for overactive bladder.' In: *World Journal of Urology* 41.5 (May 2023), pp. 1373–1379. ISSN: 14338726. DOI: 10.1007/s00345-023-04376-1.

[48] Weiwei Wang et al. 'Skin sympathetic nerve activity as a biomarker for outcomes in spontaneous intracerebral hemorrhage.' In: *Annals of Clinical and Translational Neurology* 10.7 (July 2023), pp. 1136–1145. ISSN: 2328-9503. DOI: 10.1002/acn3.51795. URL: https://onlinelibrary.wiley.com/doi/10.1002/acn3.51795.

[49] Farnoush Baghestani, Youngsun Kong, William D'Angelo, and Ki H. Chon. 'Analysis of sympathetic responses to cognitive stress and pain through skin sympathetic nerve activity and electrodermal activity.' In: *Computers in Biology and Medicine* 170 (Mar. 2024), p. 108070. ISSN: 00104825. DOI: 10.1016/j.compbiomed.2024.108070. URL: https://linkinghub.elsevier.com/retrieve/pii/S0010482524001549.

[50] A. Uradu, J. Wan, A. Doytchinova, K. C. Wright, A. Y. Lin, L. S. Chen, C. Shen, S. F. Lin, T. H. Everett, and P. S. Chen. 'Skin sympathetic nerve activity precedes the onset and termination of paroxysmal atrial tachycardia and fibrillation.' In: *Heart Rhythm* 14 (2017). DOI: 10.1016/j.hrthm.2017.03.030.

[51] Pei Zhang et al. 'Characterization of skin sympathetic nerve activity in patients with cardiomyopathy and ventricular arrhythmia.' In: *Heart Rhythm* 16.11 (Nov. 2019), pp. 1669–1675. ISSN: 15563871. DOI: 10.1016/j.hrthm.2019.06.008.

[52] T. Kusayama, J. Wan, A. Doytchinova, J. Wong, R. A. Kabir, G. Mitscher, S. Straka, C. Shen, T. H. Everett Iv, and P. S. Chen. 'Skin sympathetic nerve activity and the temporal clustering of cardiac arrhythmias.' In: (2019). DOI: 10.1172/jci.insight.125853.

[53] J. Han, M. J. Ackerman, C. Moir, C. Cai, P. L. Xiao, P. Zhang, K. A. Briske, L. R. Zheng, P. S. Chen, and Y. M. Cha. 'Left cardiac sympathetic denervation reduces skin sympathetic nerve activity in patients with long QT syndrome.' In: *Heart Rhythm* 17 (2020). DOI: 10.1016/j.hrthm.2020.03.023.

[54] Wei-Ting Sung et al. 'Alteration of Skin Sympathetic Nerve Activity after Pulmonary Vein Isolation in Patients with Paroxysmal Atrial Fibrillation.' In: *Journal of Personalized Medicine* 12.8 (Aug. 2022), p. 1286. ISSN: 2075-4426. DOI: 10.3390/jpm12081286. URL: https://www.mdpi.com/2075-4426/12/8/1286.

[55] M. J. Shen et al. 'Simultaneous recordings of intrinsic cardiac nerve activity and skin sympathetic nerve activity from human patients during the postoperative period.' In: *Heart Rhythm* 14 (2017). DOI: 10.1016/j.hrthm.2017.06.030.

[56] C. Liu, C. H. Lee, S. F. Lin, and W. C. Tsai. 'Temporal Clustering of Skin Sympathetic Nerve Activity Bursts in Acute Myocardial Infarction Patients.' In: *Frontiers in Neuroscience* 15 (2021). DOI: 10.3389/fnins.2021.720827.

[57] P. L. Xiao, C. Cai, P. Zhang, C. V. DeSimone, D. K. Ernst, Y. H. Yin, P. S. Chen, and Y. M. Cha. 'Cardiac resynchronization therapy modulates peripheral sympathetic activity.' In: *Heart Rhythm* 17 (2020). DOI: 10.1016/j.hrthm.2020.02.022.

[58] A. Kumar et al. 'Skin sympathetic nerve activity as a biomarker for syncopal episodes during a tilt table test.' In: *Heart Rhythm* 17 (2020). DOI: 10.1016/j.hrthm.2019.10.008.

[59] T. C. Huang et al. 'High skin sympathetic nerve activity in patients with recurrent syncope.' In: *Journal of Personalized Medicine* 11 (2021). DOI: 10.3390/jpm11111053.

[60] Yuan Yuan et al. 'Left cervical vagal nerve stimulation reduces skin sympathetic nerve activity in patients with drug resistant epilepsy.' In: *Heart Rhythm* 14.12 (Dec. 2017), pp. 1771–1778. ISSN: 15563871. DOI: 10.1016/j.hrthm.2017.07.035.

[61] Chen Ling Tang, Wei Chung Tsai, Jui Ying Lee, Yao Kuang Wang, Yi Hsun Chen, Yu Wei Liu, Ming Chieh Lin, Pen Tzu Fang, Yu Ling Huang, and I. Chen Wu. 'Higher pretreatment skin sympathetic nerve activity and elevated resting heart rate after chemoradiotherapy predict worse esophageal cancer outcomes.' In: *BMC Cancer* 22.1 (Dec. 2022). ISSN: 14712407. DOI: 10.1186/s12885-022-10180-8.

[62] Yike Zhang, Jing Wang, Yantao Xing, Chang Cui, Hongyi Cheng, Zhenye Chen, Hongwu Chen, Chengyu Liu, Ningning Wang, and Minglong Chen. 'Dynamics of Cardiac Autonomic Responses During Hemodialysis Measured by Heart Rate Variability and Skin Sympathetic Nerve Activity: The Impact of Interdialytic Weight Gain.' In: *Frontiers in Physiology* 13 (May 2022). ISSN: 1664042X. DOI: 10.3389/fphys.2022.890536.

[63] Xiao Liu et al. 'Skin sympathetic nerve activity and nocturnal blood pressure nondipping in patients with postural orthostatic tachycardia syndrome.' In: *Journal of Hypertension* 41.8 (Aug. 2023), pp. 1290–1297. ISSN: 0263-6352. DOI: 10.1097/HJH.0000000000003465.

[64] Hui Sophie Wang. *A Unified Dynamic Model of Electrodermal Activity*. Tech. rep. 2023.

[65] Wolfram Boucsein. *Electrodermal Activity*. Second. Springer, 2012. DOI: 10.1007/978-1-4614-1126-0.

[66] G. Bini, K. E. Hagbarth, P. Hynninen, and B. G. Wallin. 'Thermoregulatory and rhythm-generating mechanisms governing the sudomotor and vasoconstrictor outflow in human cutaneous nerves.' In: *The Journal of physiology* (1980). DOI: 10.1113/jphysiol.1980.sp013413.

[67] Robert J. Barry, Sabine Feldmann, Evian Gordon, Kathryn I. Cocker, and Chris Rennie. 'Elicitation and habituation of the electrodermal orienting response in a short interstimulus interval paradigm.' In: *International Journal of Psychophysiology* 15.3 (Nov. 1993), pp. 247–253. ISSN: 01678760. DOI: 10.1016/0167-8760(93)90008-D.

[68] Chong L. Lim, Chris Rennie, Robert J. Barry, Homayoun Bahramali, Ilario Lazzaro, Barry Manor, and Evian Gordon. 'Decomposing skin conductance into tonic and phasic components.' In: *International Journal of Psychophysiology* 25.2 (Feb. 1997), pp. 97–109. ISSN: 01678760. DOI: 10.1016/S0167-8760(96)00713-1.

[69] D.M. Alexander, C. Trengove, P. Johnston, T. Cooper, J.P. August, and E. Gordon. 'Separating individual skin conductance responses in a short interstimulus-interval paradigm.' In: *Journal of Neuroscience Methods* 146.1 (July 2005), pp. 116–123. ISSN: 01650270. DOI: 10.1016/j.jneumeth.2005.02.001.

[70] Mathias Benedek and Christian Kaernbach. 'A continuous measure of phasic electrodermal activity.' In: *Journal of Neuroscience Methods* 190.1 (June 2010), pp. 80–91. ISSN: 01650270. DOI: 10.1016/j.jneumeth.2010.04.028.

[71] Mathias Benedek and Christian Kaernbach. 'Decomposition of skin conductance data by means of nonnegative deconvolution.' In: *Psychophysiology* (Mar. 2010). ISSN: 00485772. DOI: 10.1111/j.1469-8986.2009.00972.x.

[72] Dominik R. Bach. 'A head-to-head comparison of SCRalyze and Ledalab, two model-based methods for skin conductance analysis.' In: *Biological Psychology* 103 (Dec. 2014), pp. 63–68. ISSN: 03010511. DOI: 10.1016/j.biopsycho.2014.08.006.

[73] Alberto Greco, Gaetano Valenza, Antonio Lanata, Enzo Scilingo, and Luca Citi. 'cvxEDA: a Convex Optimization Approach to Electrodermal Activity Processing.' In: *IEEE Transactions on Biomedical Engineering* 63.4 (Apr. 2016), pp. 1–1. ISSN: 0018-9294. DOI: 10.1109/TBME.2015.2474131. URL: http://ieeexplore.ieee.org/document/7229284/.

[74] Alberto Greco, Antonio Lanata, Gaetano Valenza, Enzo Pasquale Scilingo, and Luca Citi. 'Electrodermal activity processing: A convex optimization approach.' In: *2014 36th Annual International Conference of the IEEE Engineering in Medicine and Biology Society*. IEEE, Aug. 2014, pp. 2290–2293. ISBN: 978-1-4244-7929-0. DOI: 10.1109/EMBC.2014.6944077.

[75] Mega Electronics Ltd. *Biomonitor ME6000 Multisignal system*. Tech. rep. Kuopio, Finland.

[76] Shimmer. *GSR+ User Guide*. Tech. rep. Dublin, Ireland, 2018.

[77] Wikipedia. *Einthoven's triangle*. URL: https://en.wikipedia.org/wiki/Einthoven%27s_triangle.

[78] *Empatica E4*. URL: https://www.empatica.com/en-gb/research/e4/.

[79] TMSi. *REFA amplifier*. URL: https://www.tmsi.com/products/refa/.

[80] Danilo Ricciardi et al. 'Impact of the high-frequency cutoff of bandpass filtering on ECG quality and clinical interpretation: A comparison between 40Hz and 150Hz cutoff in a surgical preoperative adult outpatient population.' In: *Journal of Electrocardiology* 49.5 (Sept. 2016), pp. 691–695. ISSN: 00220736. DOI: 10.1016/j.jelectrocard.2016.07.002.

[81] Jiapu Pan and Willis J. Tompkins. 'A Real-Time QRS Detection Algorithm.' In: *IEEE Transactions on Biomedical Engineering* BME-32.3 (Mar. 1985), pp. 230–236. ISSN: 0018-9294. DOI: 10.1109/TBME.1985.325532.

[82] Hooman Sedghamiz. *Complete Pan Tompkins Implementation ECG QRS detector*. Apr. 2018. URL: https://nl.mathworks.com/matlabcentral/fileexchange/45840-complete-pan-tompkins-implementation-ecg-qrs-detector.

[83] F.S. Grodins. *Control Theory and Biological Systems*. Ed. by Columbia University Press. New York, 1963.

[84] Md Rafiul Amin and Rose T Faghih. *Identification of Sympathetic Nervous System Activation from Skin Conductance: A Sparse Decomposition Approach with Physiological Priors*. Tech. rep. 2020.

[85] Lingzhong Meng, Weifeng Yu, Tianlong Wang, Lina Zhang, Paul M. Heerdt, and Adrian W. Gelb. 'Blood Pressure Targets in Perioperative Care.' In: *Hypertension* 72.4 (Oct. 2018), pp. 806–817. ISSN: 0194-911X. DOI: 10.1161/HYPERTENSIONAHA.118.11688.

[86] Rachel Nall, Heather Hobbs, and Elaine Luo. *Understanding Mean Arterial Pressure*. 2023. URL: https://www.healthline.com/health/mean-arterial-pressure#normal-map.

[87] Deb Hipp and Ardeshir Hashmi. *Normal Resting Heart Rate By Age (Chart)*. 2024. URL: https://www.forbes.com/health/wellness/normal-heart-rate-by-age/.

[88] Hatem Ghouili, Zouhaier Farhani, Sofiane Amara, Soukaina Hattabi, Amel Dridi, Noomen Guelmami, Anissa Bouassida, Nicholas Braghazzi, and Ismail Dergaa. 'Normative data in resting and maximum heart rates and a prediction equation for young tunisian soccer

players: A cross-sectional study.' In: *EXCLI Journal* 22 (2023), pp. 670–680. ISSN: 16112156. DOI: 10.17179/excli2023-6215.

[89] MathWorks. *Optimizing Nonlinear Functions*. URL: OptimizingNonlinearFunctions.

[90] Jeffrey C. Lagarias, James A. Reeds, Margaret H. Wright, and Paul E. Wright. 'Convergence Properties of the Nelder–Mead Simplex Method in Low Dimensions.' In: *SIAM Journal on Optimization* 9.1 (Jan. 1998), pp. 112–147. ISSN: 1052-6234. DOI: 10.1137/S1052623496303470.

[91] Jade Yu Cheng and Thomas Mailund. *An iteration of the Nelder-Mead method over two-dimensional space*. Mar. 2015. URL: https://en.wikipedia.org/wiki/File:An-iteration-of-the-Nelder-Mead-method-over-two-dimensional-space-showing-point-p-min.png.

[92] Wikipedia. *Coefficient of determination*. URL: https://en.wikipedia.org/wiki/Coefficient_of_determination.

[93] Wikipedia. *Root Mean Square Deviation*. URL: https://en.wikipedia.org/wiki/Root_mean_square_deviation.

[94] S.A. Otto. *How to normalize the RMSE [Blog post]*. URL: https://www.marinedatascience.co/blog/2019/01/07/normalizing-the-rmse/#.

[95] Nicolle van Rijswijk. *Sampling frequency*. TMSi Support. (On 07/08/2024).

[96] D. J. van der Mee, M. J. Gevonden, J. H.D.M. Westerink, and E. J.C. de Geus. 'Validity of electrodermal activity-based measures of sympathetic nervous system activity from a wrist-worn device.' In: *International Journal of Psychophysiology* 168 (Oct. 2021), pp. 52–64. ISSN: 18727697. DOI: 10.1016/j.ijpsycho.2021.08.003.

A

APPENDIX

A.1 STUDY 2023

This section gives the individual results for Study 2023, Tertoolen's dataset. Furthermore, the mean results are provided for the first VM.

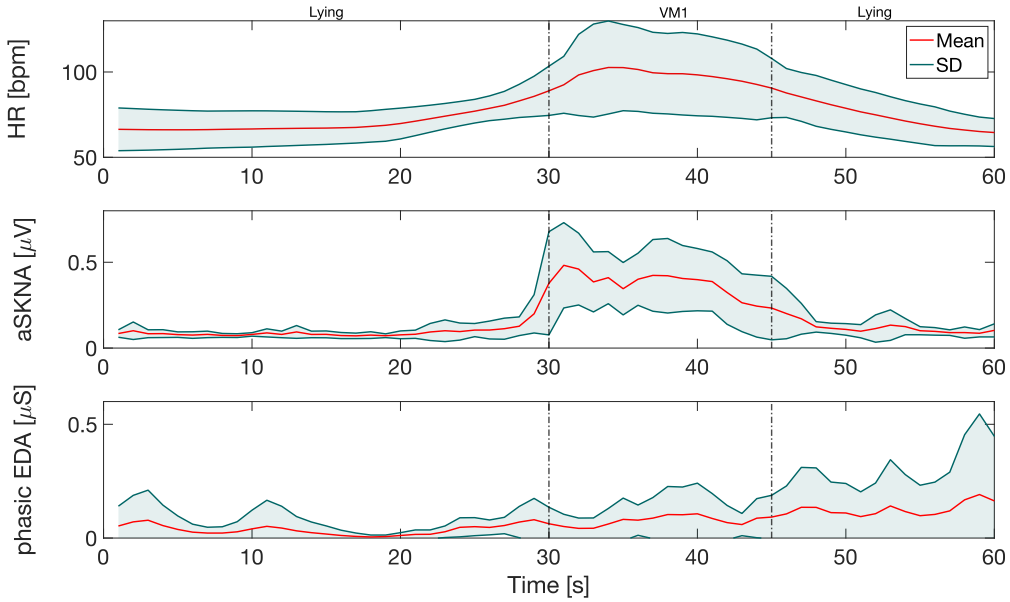

Figure 15: Mean (red) measured heart rate, aSKNA, and the phasic component of EDA for Study 2023, Tertoolen's dataset, shown over time, where the VM is performed at t = 30 s for 15 s. During this epoch, the subject lay down and performed the first VM. The green areas indicate the standard deviation.

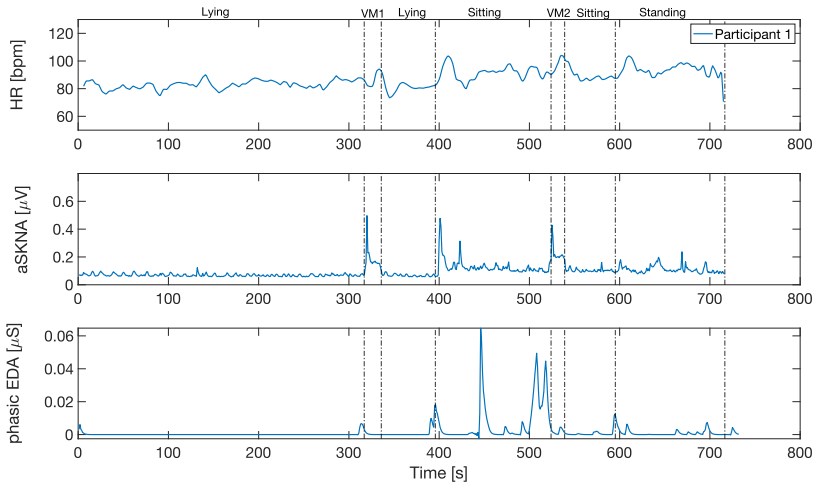

Figure 16: Heart rate, aSKNA, and the phasic component of EDA over the entire timeline for participant 1 of Study 2023, Tertoolen's dataset. Activity phases are indicated in the text above the graph.

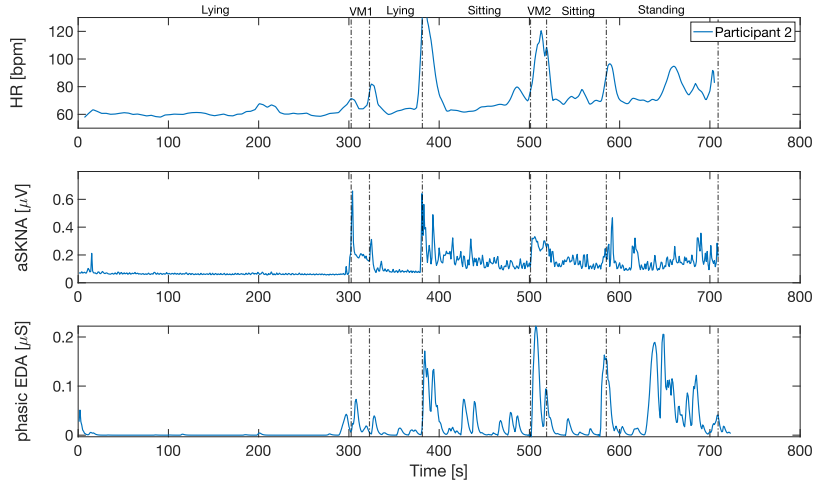

Figure 17: Participant 2 of Study 2023, Tertoolen's dataset.

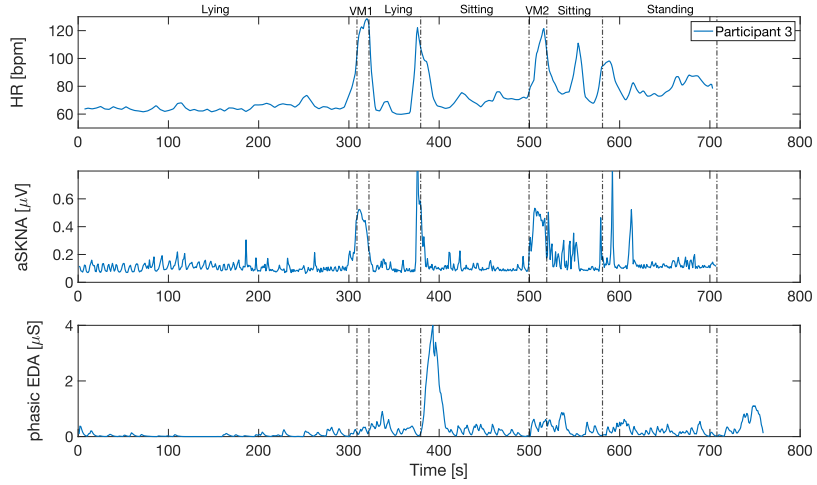

Figure 18: Participant 3 of Study 2023, Tertoolen's dataset.

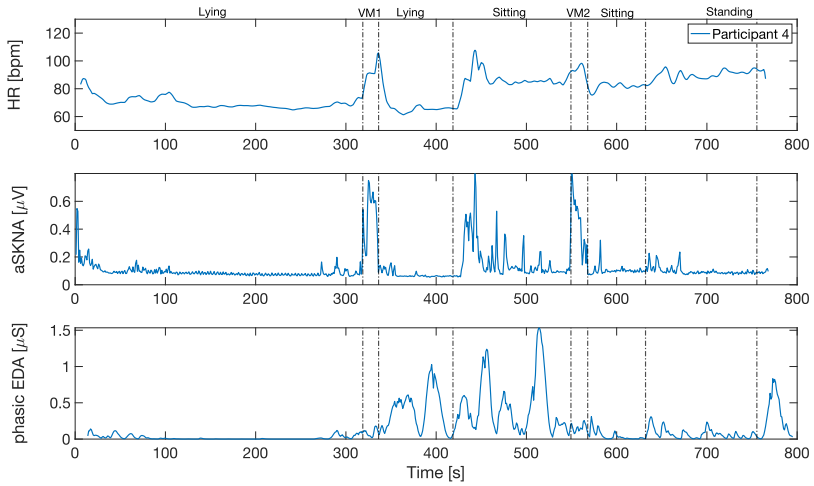

Figure 19: Participant 4 of Study 2023, Tertoolen's dataset.

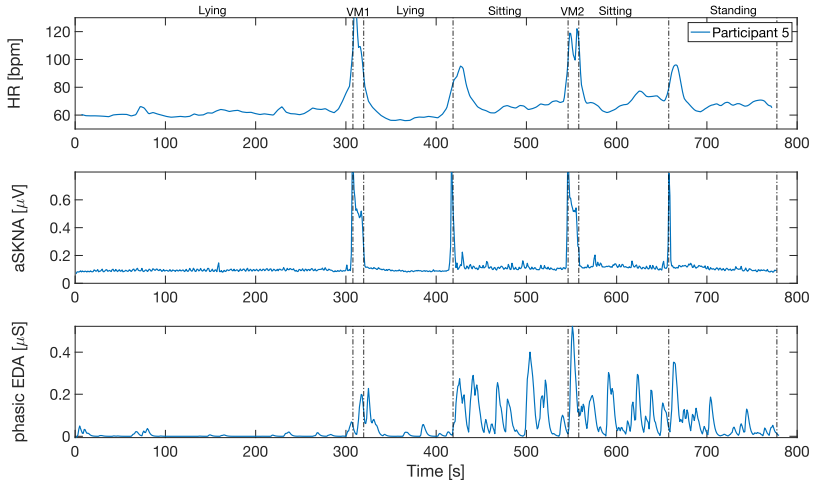

Figure 20: Participant 5 of Study 2023, Tertoolen's dataset.

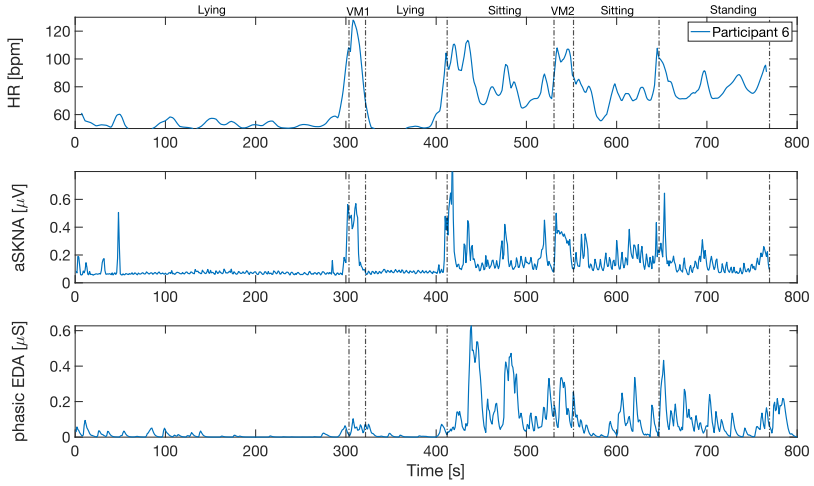

Figure 21: Participant 6 of Study 2023, Tertoolen's dataset.

A.2 STUDY 2024

Below, additional results are given on Study 2024, the dataset obtained during this research.

Table 9: Individual subject characteristics for Study 2024.

Participant	Sex	Age [year]	Weight [kg]	Height [cm]	BMI [kg/m²]
1	Female	23	54.6	170	18.9
2	Male	24	83.5	187	23.9
3	Male	23	84.5	175	27.6
4	Male	28	66.5	168	23.6
5	Male	49	70.7	186	20.4
6	Male	29	92.2	178	29.1
7	Female	23	65.5	177	20.9
8	Male	23	73.4	183	21.9
9	Male	23	77.2	187	22.1
10	Female	23	61.9	169.5	21.5

A.2.1 *Sampling frequency 1250 Hz*

This subsection provides the results for an assumed sampling rate of 1250 Hz.

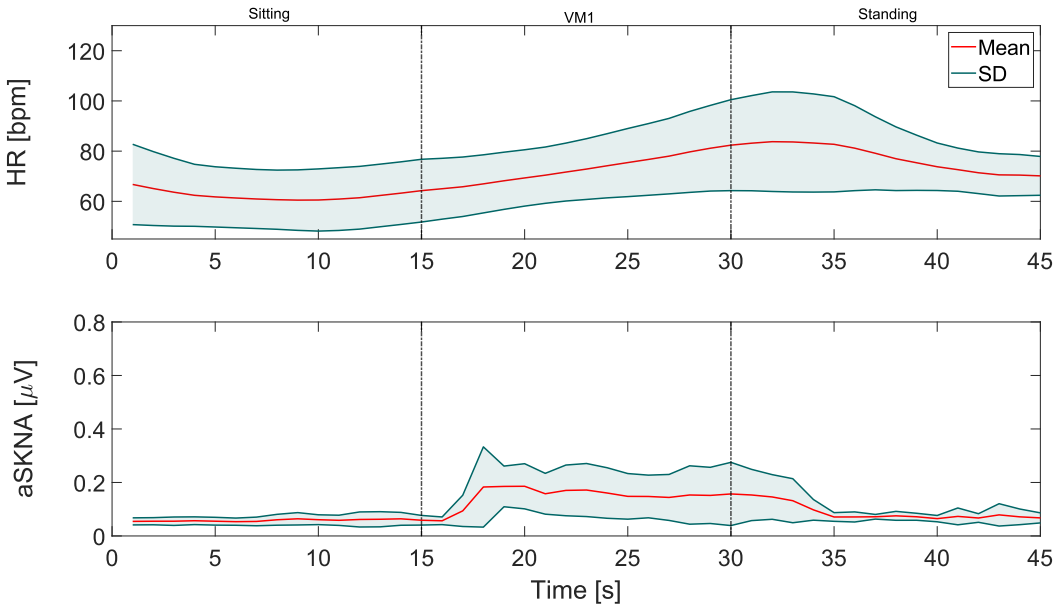

Figure 22: Mean (red) measured heart rate, aSKNA, and the phasic component of EDA for Study 2024 shown over time, where the VM is performed at t = 15 s for 15 s. During this epoch, the subject sat, performed the first VM, and then stood up. The green areas indicate the standard deviation.

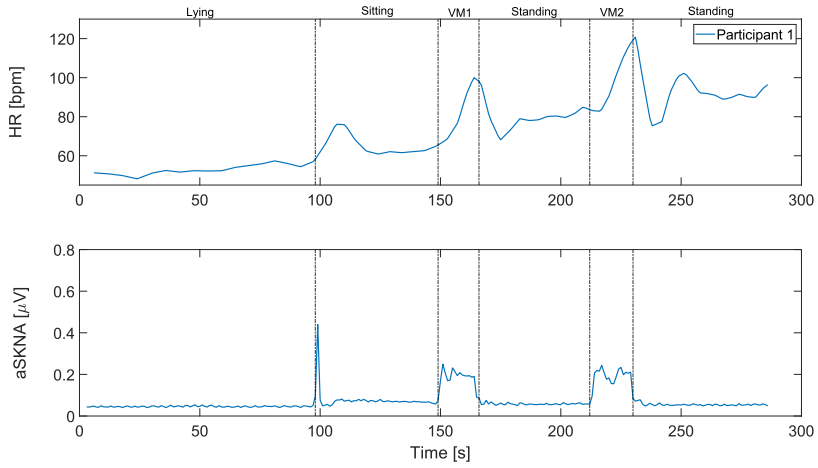

Figure 23: Participant 1 of Study 2024.

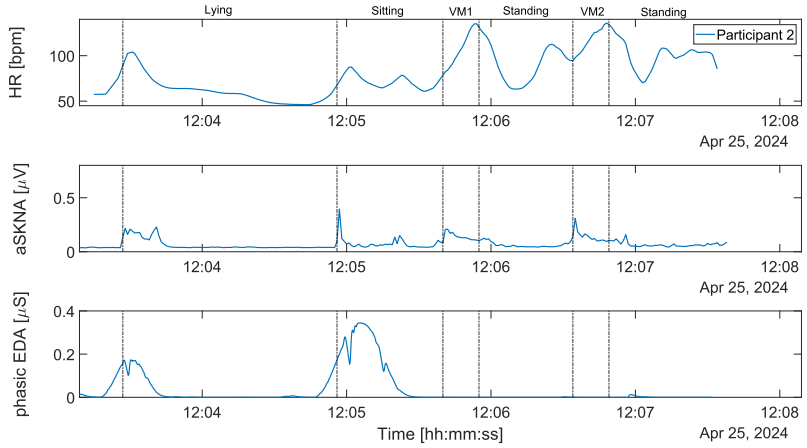

Figure 24: Participant 2 of Study 2024.

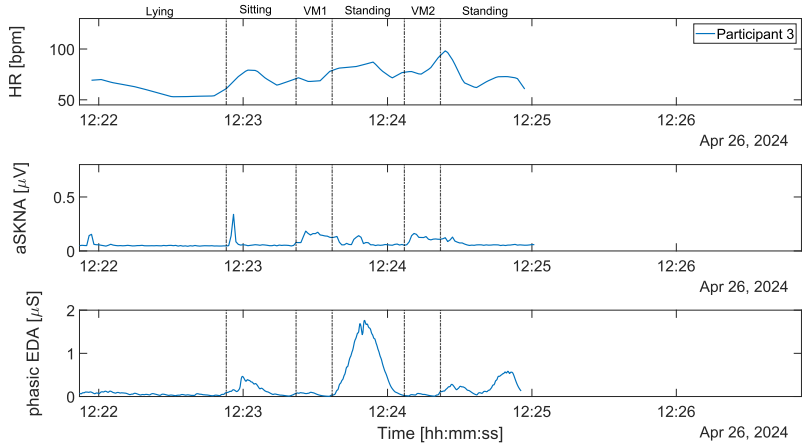

Figure 25: Participant 3 of Study 2024.

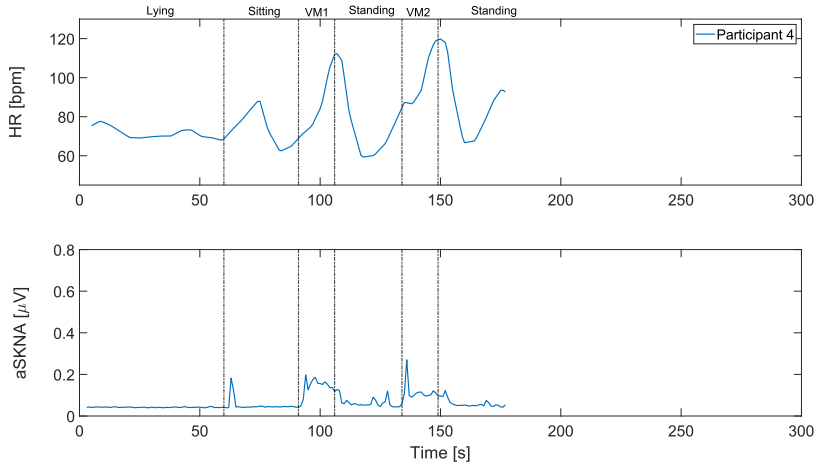

Figure 26: Participant 4 of Study 2024.

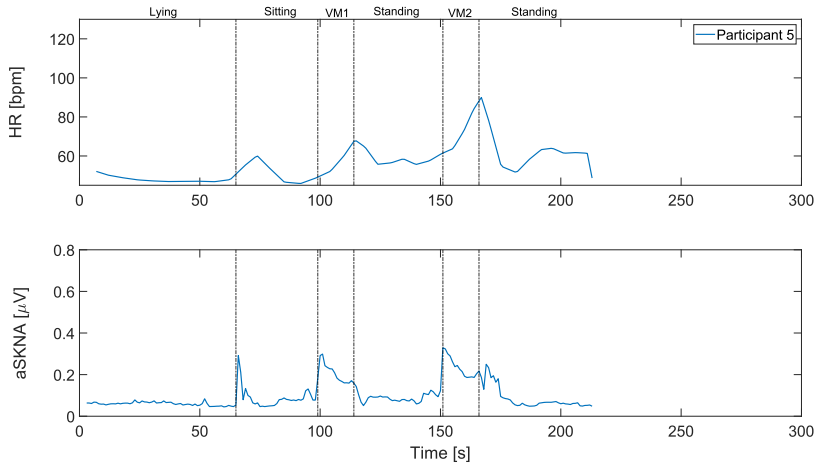

Figure 27: Participant 5 of Study 2024.

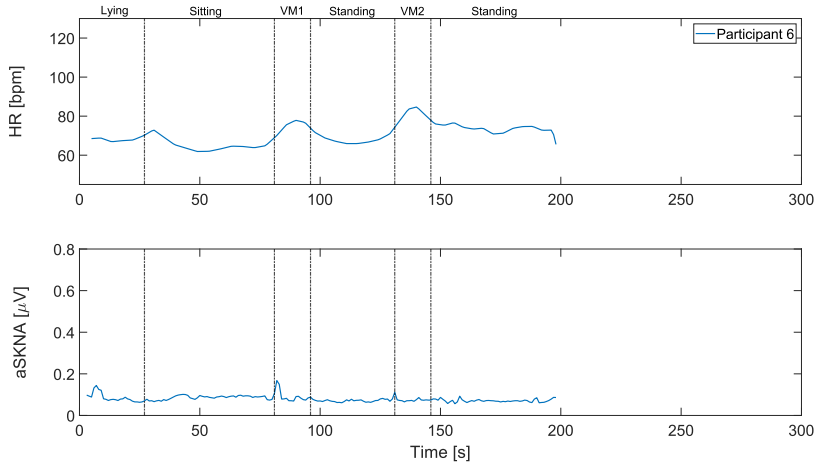

Figure 28: Participant 6 of Study 2024.

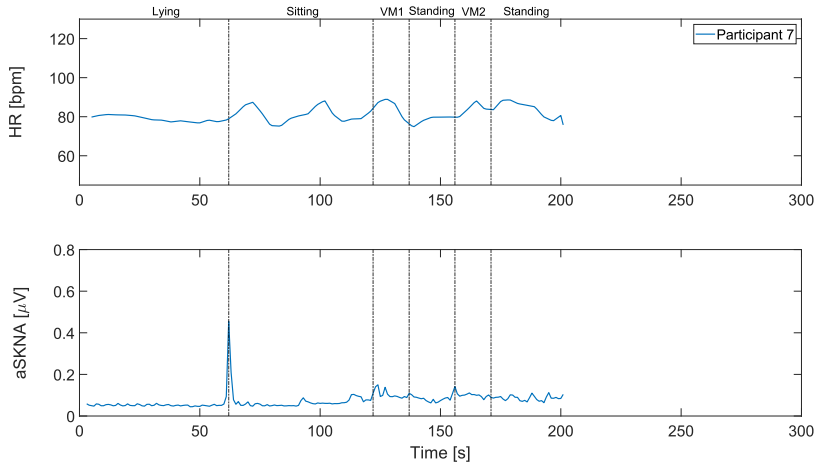

Figure 29: Participant 7 of Study 2024.

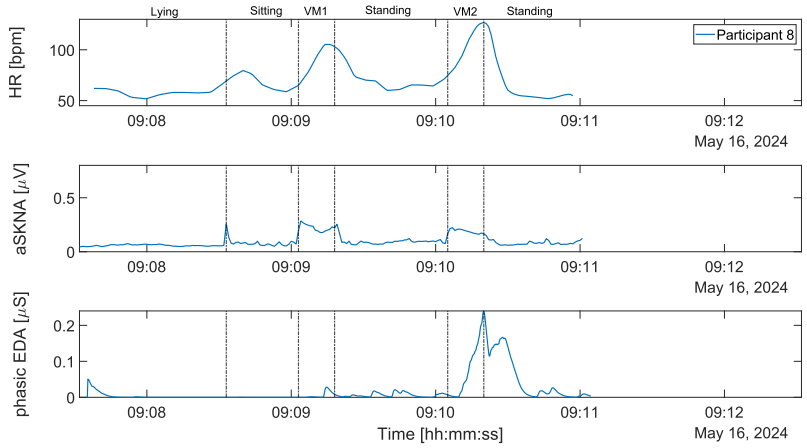

Figure 30: Participant 8 of Study 2024.

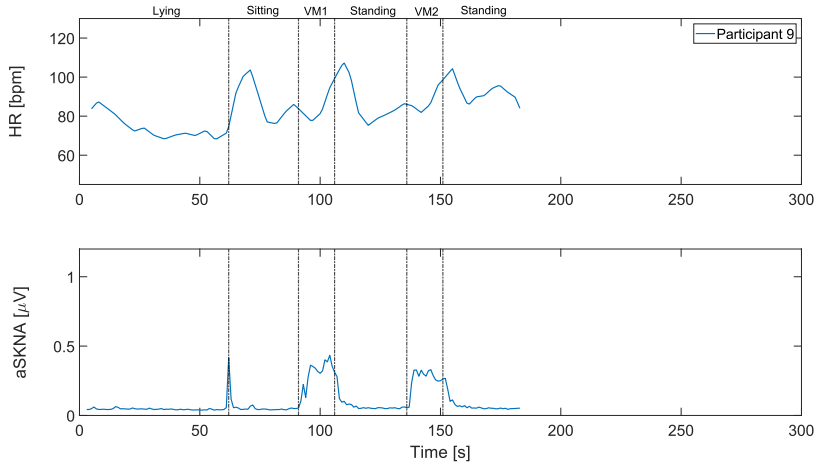

Figure 31: Participant 9 of Study 2024.

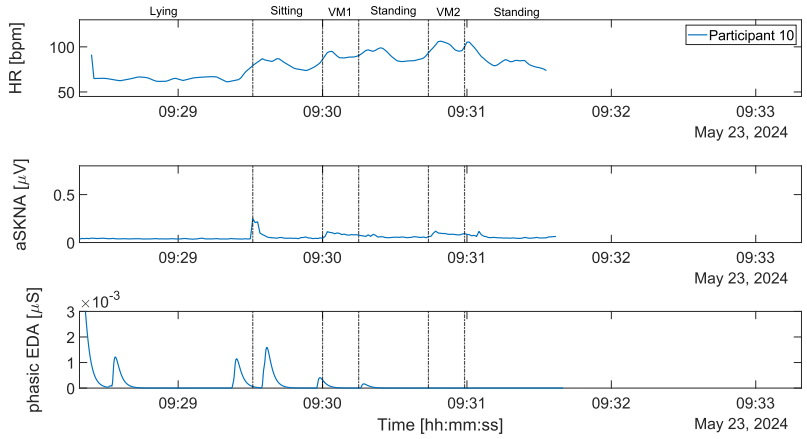

Figure 32: Participant 10 of Study 2024 (fs = 1250 Hz).

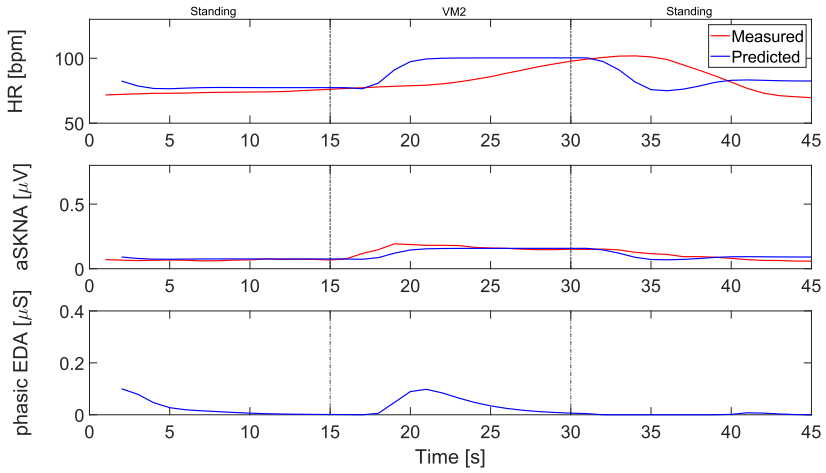

Figure 33: Predicted (blue) and measured (red) mean heart rate and aSKNA, and the predicted phasic component of EDA over time. The measured data is from Study 2024. The subject was standing and performed the Valsalva Manoeuvre between 15 and 30 s.

A.2.2 *Sampling frequency 2048 Hz*

These are the results with a sampling frequency of 2048 Hz, which we had 'set' as a sampling rate.

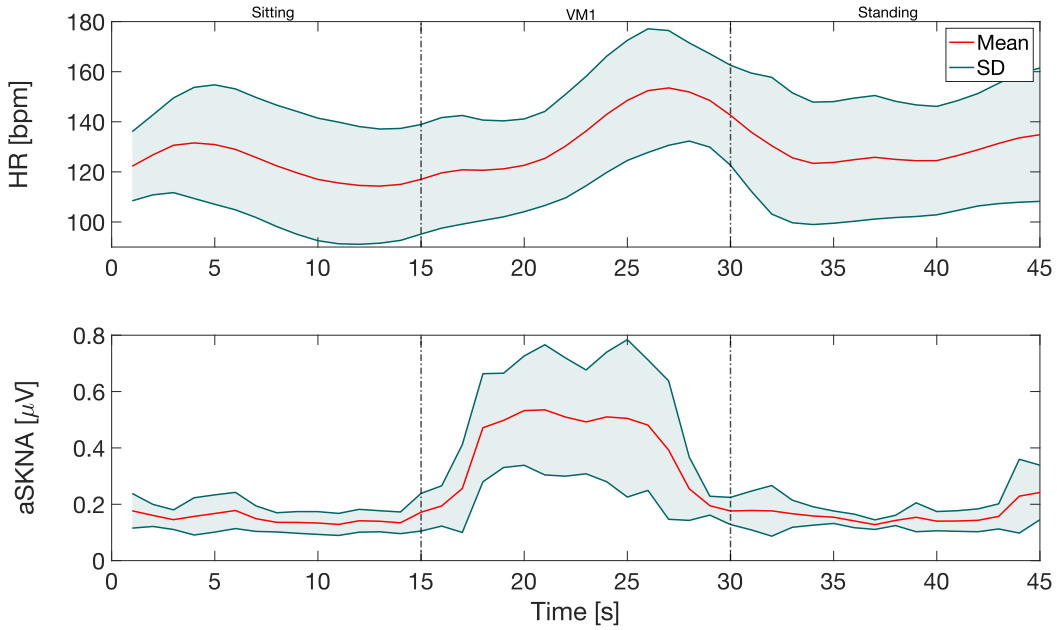

Figure 34: Mean (red) measured heart rate, aSKNA, and the phasic component of EDA for Study 2024 shown over time, where the VM is performed at t = 15 s for 15 s. During this epoch, the subject sat, performed the first VM, and then stood up. The green areas indicate the standard deviation.

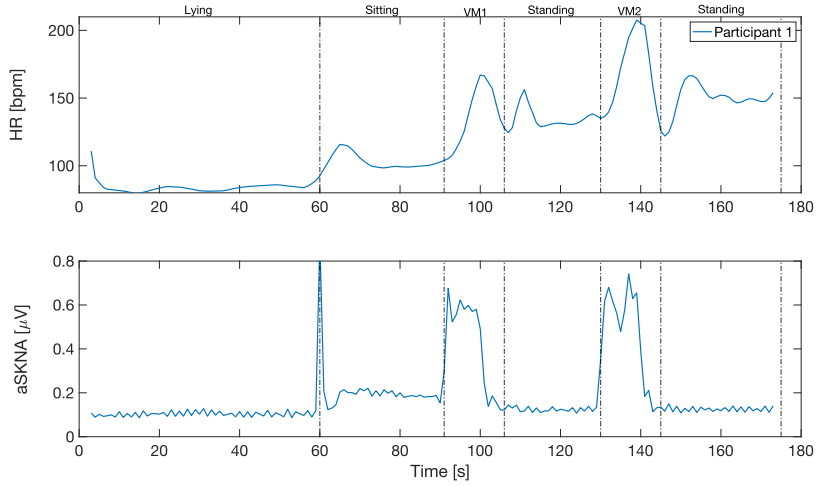

Figure 35: Participant 1 of Study 2024.

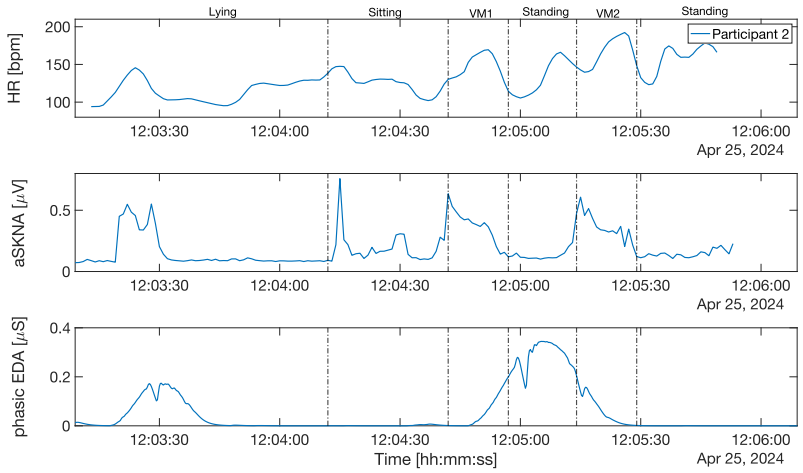

Figure 36: Participant 2 of Study 2024.

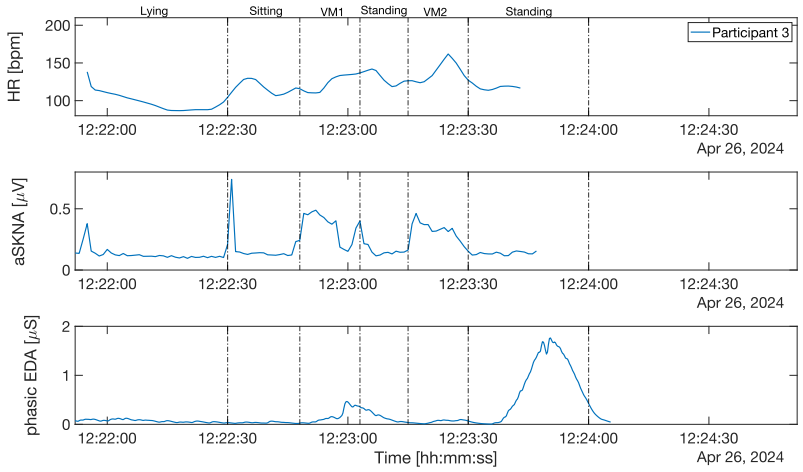

Figure 37: Participant 3 of Study 2024.

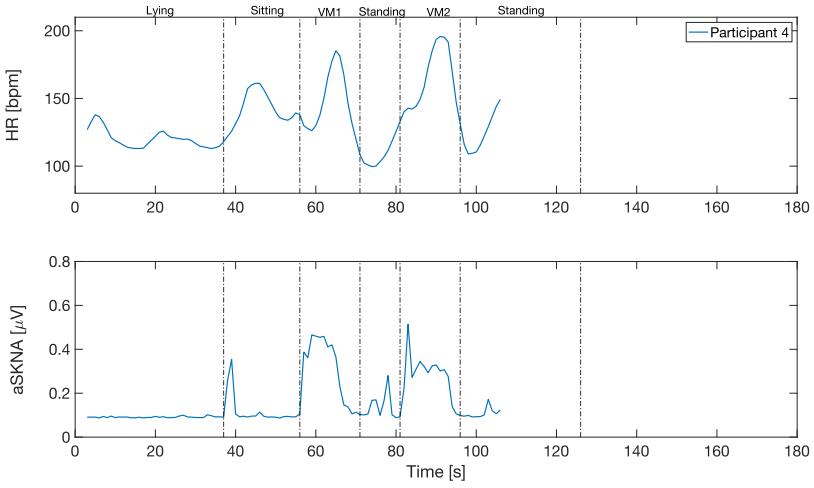

Figure 38: Participant 4 of Study 2024.

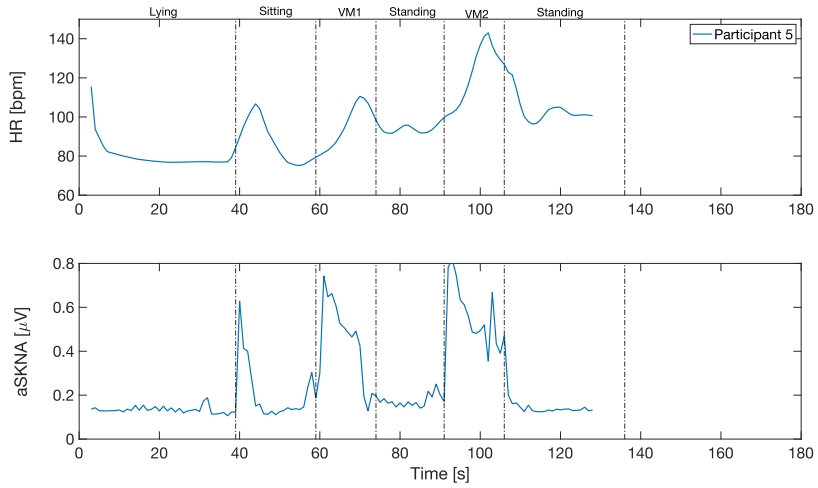

Figure 39: Participant 5 of Study 2024.

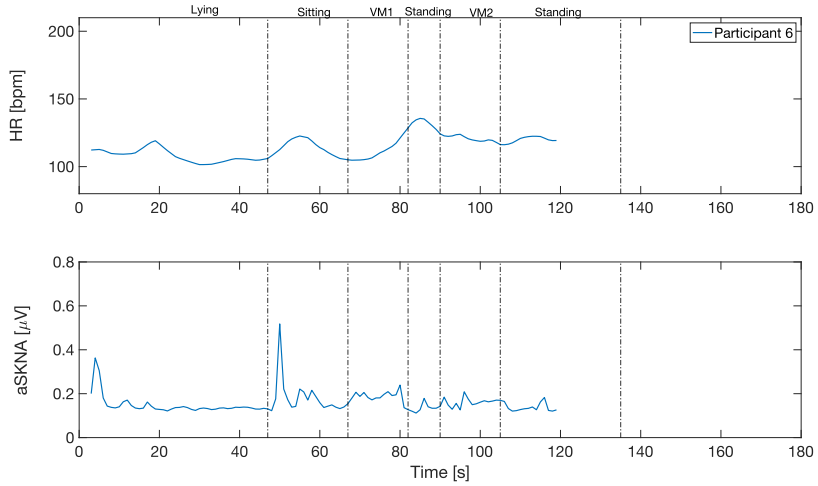

Figure 40: Participant 6 of Study 2024.

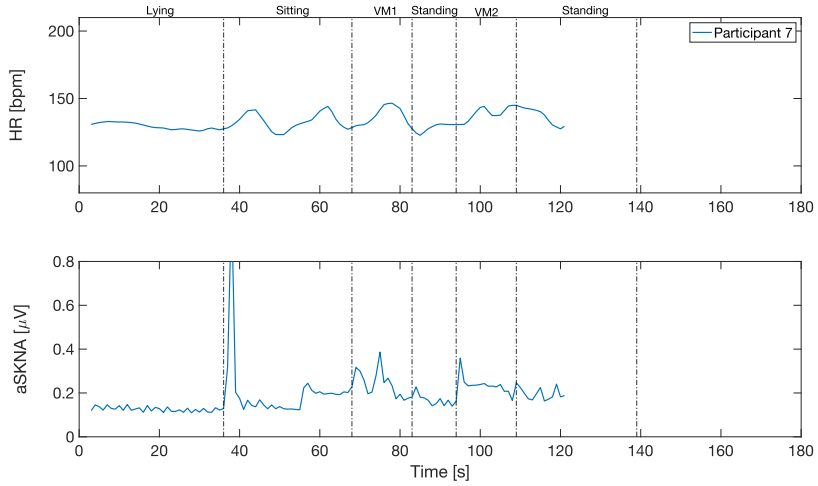

Figure 41: Participant 7 of Study 2024.

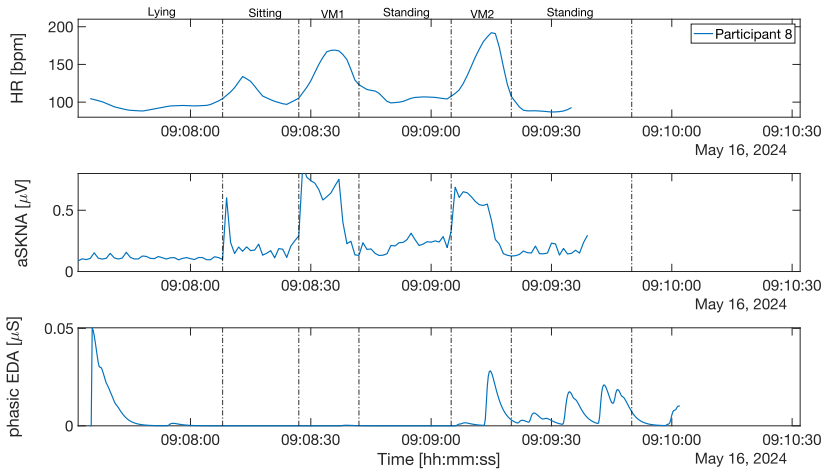

Figure 42: Participant 8 of Study 2024.

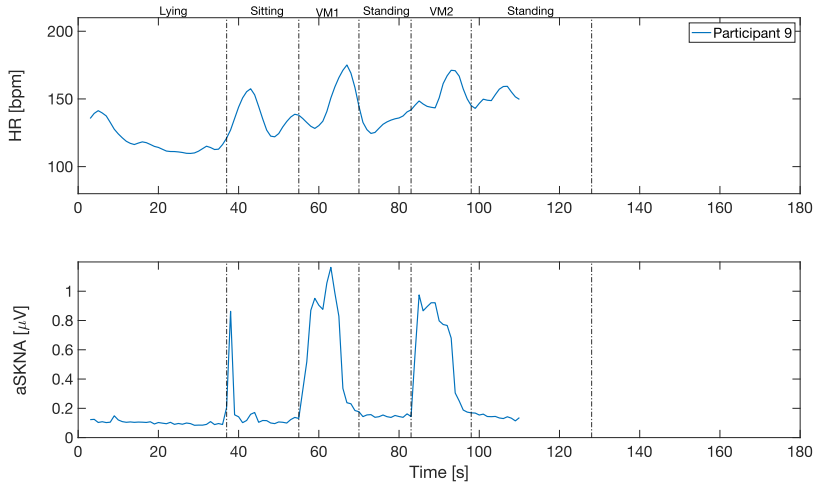

Figure 43: Participant 9 of Study 2024.

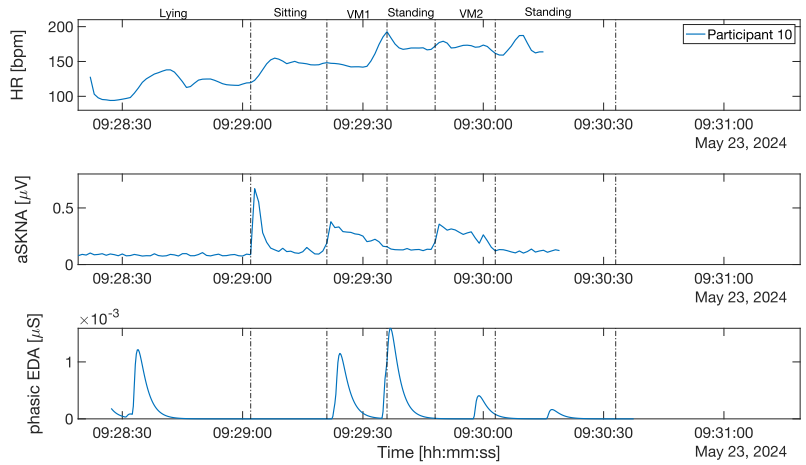

Figure 44: Participant 10 of Study 2024.

A.2.3 *Refa specifications*

95-0120-2000-0, Refa8-16e 20000Hz

Type	**Refa8-16e**
REF code	95-0120-2000-0
Unipolar ExG inputs (EEG, ECG, EOG, EMG etc):	
Number	16
RMS Noise	< 1 μV (@ lowest sample frequency)
Gain	26.55 x
Input signal difference	-150 mV to +150 mV (@ 0 V common signal)
Input common mode range	-2 V to +2 V (@ 0 V differential signal)
Input impedance	> 100 MΩ
CMRR	> 90 dB
Connectors	active shielded micro coax per channel subD37 female unshielded per 32 channels
Digital input	
Input turn-on current	2 mA @ 3 V input, max. input = 5 V
Isolation	> 4000 V, by means of optocoupler (H11L1)
Connector	8 bit via DB25 female, shared first bit via BNC female
Sampling:	
Number of channels	16 channels simultaneously
Resolution	24 bits, ExG 18.39 nV per bit
Sample frequency	20000 Hz, 10000 Hz, 5000 Hz, 2500 Hz, 1250 Hz

Figure 45: Specifications of the Refa with 16 channels and maximal sampling frequency of 20 kHz.